# Cognitive Radio Empowered Smart Grid

Zhaoyue Xia, *Member, IEEE*, Quan Zhou, *Senior Member, IEEE*, Mohammad Shahidehpour, *Life Fellow, IEEE*, and Zhikang Shuai, *Senior Member, IEEE*

***Abstract*—The increasing reliance on distributed energy resources and the need for resilient grid operation in vulnerable or infrastructure-limited areas have led to a move from wired connections to wireless communication in smart grids. Despite significant progress in wireless resource management, a fundamental question remains: how can communication resource management directly influence and enhance the operation of the smart grid itself? To address this challenge, this paper proposes a cognitive radio empowered smart grid (CRESG) architecture, where distributed generators (DGs) interact with a main controller (MC) over adaptive wireless links. To capture the impact of short-packet transmission delay and error probability on control performance, a finite blocklength (FBL) regime is adopted within the context of ultra-reliable low-latency communication (URLLC). Based on this architecture, a coupled multi-objective optimization framework is developed, integrating wireless communication design with finite-time stability constraints from smart grid dynamics. To evaluate the performance of the proposed architecture, two representative smart grid scenarios are examined: (i) satellite-assisted remote control of offshore wind turbines and (ii) wireless transmission of generation control signals from a remote control center to multiple distributed renewable energy resources (RERs). The simulation results consistently demonstrate that the proposed architecture effectively balances latency, reliability, and communication-control cost under diverse grid operation constraints, thereby validating its adaptability to smart grids supported by advanced wireless communication technologies.**

***Index Terms*—Smart grid, cognitive radio, on-demand communication service, power control and communication co-design.**

## I. Introduction

THE rapid expansion of distributed RERs, including offshore wind farms, desert photovoltaic stations, and clustered hydropower plants, is driving a fundamental transformation in modern smart grid architectures. These geographically dispersed and environmentally diverse resources introduce new challenges to system coordination and stability. In addition, emerging power facilities in extreme regions, such as polar research stations and remote islands, further increase the demand for reliable communication links to enable real-time monitoring, coordinated control, and secure data exchange. Although stable under normal conditions, traditional wired infrastructures are often costly to deploy especially for large-scale distributed renewable power systems and vulnerable to faults caused by natural disasters and harsh climates. In contrast, wireless communication offers superior resilience and flexibility, enabling rapid deployment and reconfiguration even in challenging environments. This makes wireless networks particularly suitable for emergency control, remote operation, and fast restoration in large-scale renewable and geographically distributed power systems.

As wireless communication plays an increasingly important role in modern power systems, the limitation of communication resources is emerging as a critical bottleneck. The rapid proliferation of renewable generators, distributed controllers, and sensing devices generates massive and diverse traffic over shared wireless channels. Without effective coordination, simultaneous access by numerous nodes can easily lead to spectrum congestion, latency increase, and data loss. These issues directly deteriorate system stability, damping performance, and economic dispatch efficiency. In such dense and dynamic communication environments, it is essential to provide **on-demand services** so that each electrical apparatus can obtain transmission opportunities consistent with its control priority and practical necessity. Achieving this goal requires dynamic and adaptive communication resource management capable of adjusting bandwidth, power, and access in real time according to operational needs. In summary, demand-driven resource management is significant for wireless communication to fully support the stringent requirements for reliability, resilience, and scalability in future (distributed) smart grids.

Recent years have witnessed a growing body of work on integrating on-demand wireless communication schemes into smart grids to enable resilient, flexible, and cost-efficient operation in cyber-physical energy systems. URLLC has been identified as a key enabler for control-centric applications, where millisecond-level response and high reliability are critical for energy trading, demand response and frequency regulation in smart grid environments [1], [2], [3]. Studies have demonstrated that by leveraging tailored scheduling, data-driven and beamforming techniques, URLLC can maintain stable operation under rapidly changing load and generation profiles, even in highly distributed microgrid clusters. Conventional wireless communication schemes in smart grids (e.g., WiMAX, ZigBee, power line communication) rely on

Received 14 August 2025; revised 7 November 2025; accepted 4 December 2025. Date of publication 9 December 2025; date of current version 23 April 2026. This work was supported in part by the National Key Research and Development Program of China under Grant 2024YFB2409100, in part by the General Project of National Natural Science Foundation of China under Grant 52477091, and in part by the Science and Technology Innovation Program of Hunan Province under Grant 2024RC1038. Paper no. TSG-01639-2025. *(Corresponding author: Quan Zhou.)*

Zhaoyue Xia, Quan Zhou, and Zhikang Shuai are with the College of Electrical and Information Engineering, Hunan University, Changsha 410082, China (e-mail: xiazhy@hnu.edu.cn; zquan@hnu.edu.cn; szk@hnu.edu.cn).

Mohammad Shahidehpour is with Galvin Center for Electricity Innovation, Illinois Institute of Technology, Chicago, IL 60616 USA (e-mail: ms@iit.edu).

Digital Object Identifier 10.1109/TSG.2025.3642174

1949-3053 © 2025 IEEE. All rights reserved, including rights for text and data mining, and training of artificial intelligence and similar technologies. Personal use is permitted, but republication/redistribution requires IEEE permission.
See https://www.ieee.org/publications/rights/index.html for more information.

Authorized licensed use limited to: HUNAN UNIVERSITY. Downloaded on September 25,2026 at 04:35:22 UTC from IEEE Xplore. Restrictions apply.

static resource allocation and lack adaptability for large-scale, dynamic networks. By contrast, cognitive radio (CR) introduces dynamic spectrum management, enabling efficient resource utilization and has the potential for next-generation smart grids. CR and wireless communication technologies have also been explored for smart grids, enabling dynamic spectrum sensing, interference mitigation, and adaptive channel allocation to support the high-priority traffic of grid control tasks without compromising coexisting services in [4] and [5]. Nevertheless, these frameworks do not sufficiently address the physical-layer interactions between communication and power systems. By contrast, recent studies have tightened the loop between communication and grid control. For instance, bandwidth-conscious event-based secondary frequency regulation has been investigated by adapting automatic generation control (AGC) broadcast rates to real-time bandwidth occupancy and co-designs the controller with an event trigger to save spectrum [6]. At the distribution level, delay-aware microgrid control advances [7] propose distributed estimators and voltage controllers that precisely recover the average voltage and enforce proportional reactive power sharing under bounded and time-varying delays. Beyond link-level control, a two-timescale mobile-edge computing framework [8] has been applied to jointly manage wireless offloading, base station (BS) energy trading with the smart grid, and CPU configurations, minimizing overall long-term system cost. At the restoration layer, a post-disaster robust restoration scheme is proposed [9], which optimizes cyber rerouting to reconnect offline field devices and accelerate physical restoration, explicitly exploiting network connectivity to heal the control plane after extreme events. In [10], a sensing-transmission-computing-control integrated optimization problem is investigated aimed to minimize the overall voltage deviation in smart grids. The effects of wireless transmission latency on the performance of a wireless communication supported high renewable energy penetrated power system is studied in [11]. In addition, a cross-domain power-communication collaborative control optimization problem is investigated in [12] to achieve accurate false data injection attack sensing, secure data transmission and trust and delay-weighted consensus control. For further related research, the readers are referred to [13], [14], [15], [16], and [17]. In summary, these recent works confirm that grid performance is communication-limited (in terms of delay and reliability), and adaptive communication resource management is economically valuable across normal and emergency operations.

Current CR-based frameworks for smart grids primarily focus on linking the quality of service (QoS) experienced by mobile users with the runtime control of nearby grid assets through the BS or providing secure communications for operations of smart grid assets. However, a key challenge still remains: **how can communication resource management directly influence and enhance the operation of the smart grid itself?** This work addresses that challenge by establishing a general framework in which wireless communication resource management is deeply integrated into the control of a distributed power system. To this end, we propose a novel architecture, termed the CR empowered smart grid (CRESG), which explicitly couples adaptive resource access with stability-critical grid control to achieve cost-efficient, reliable, and resilient smart grid operation. The defining characteristics of the proposed CRESG are two-fold. First, it relies on short-packet transmission, in which concise control signals are delivered under strict latency and reliability constraints, aligning with the practical requirements of URLLC in modern grid operations. Second, the communication terminal equipped at the MC is capable of acquiring channel state information (CSI) for each MC-DG link. This enables dynamic time-frequency resource management and access control to adaptively satisfy QoS demands in smart grid operations. In this work, CR is not restricted to traditional spectrum sensing and access, but expanded to comprehensive power grid and communication network status cognition, based on which communication resources are adaptively managed.

In short-packet transmission, the error probability cannot be made arbitrarily small independently of the achievable data rate when the bandwidth, signal-to-noise ratio (SNR), and transmission delay are fixed. This behavior fundamentally deviates from the predictions of the classical Shannon paradigm [18]. In particular, both transmission delay and error probability directly affect grid stability. However, increasing communication bandwidth or transmit power to reduce latency and error probability is not always feasible, as both factors significantly contribute to the overall operational cost. To address these challenges, we develop a cross-system optimization framework that couples the inherent stability constraints of the smart grid with the adaptive management of wireless communication resources. By modeling the control system using nonlinear time-delay dynamics and adopting an FBL regime for the communication model, we derive tractable expressions that link delay, error probability, and data rate. Based on these relationships, a constrained optimization problem is formulated to minimize the joint communication-power cost. The performance of CRESG is further assessed with application to satellite-assisted control of offshore wind turbines and remote control of RERs, demonstrating how adaptive resource allocation can achieve both cost-efficient and low-latency reliable control in smart grids. The main contributions of this paper are summarized as follows.

- Unlike existing works that treat communication and control as loosely coupled layers, the proposed architecture explicitly links URLLC performance in the FBL regime with finite-time stability requirements in distributed smart grid control. This integration enables modeling of the impact of latency and error probability on grid stability, forming a unified framework for cost-aware and control-dependent communication resource management.
- The paper develops a tractable formulation that jointly optimizes wireless resource allocation and control-induced operational cost, subject to URLLC latency and reliability constraints. The framework captures the hybrid (possibly non-convex) cost tradeoff between communication resource rental and stability-related grid operational expenditure (with respect to transmission latency), providing a systematic approach to balance QoS and

Authorized licensed use limited to: HUNAN UNIVERSITY. Downloaded on September 25,2026 at 04:35:22 UTC from IEEE Xplore. Restrictions apply.

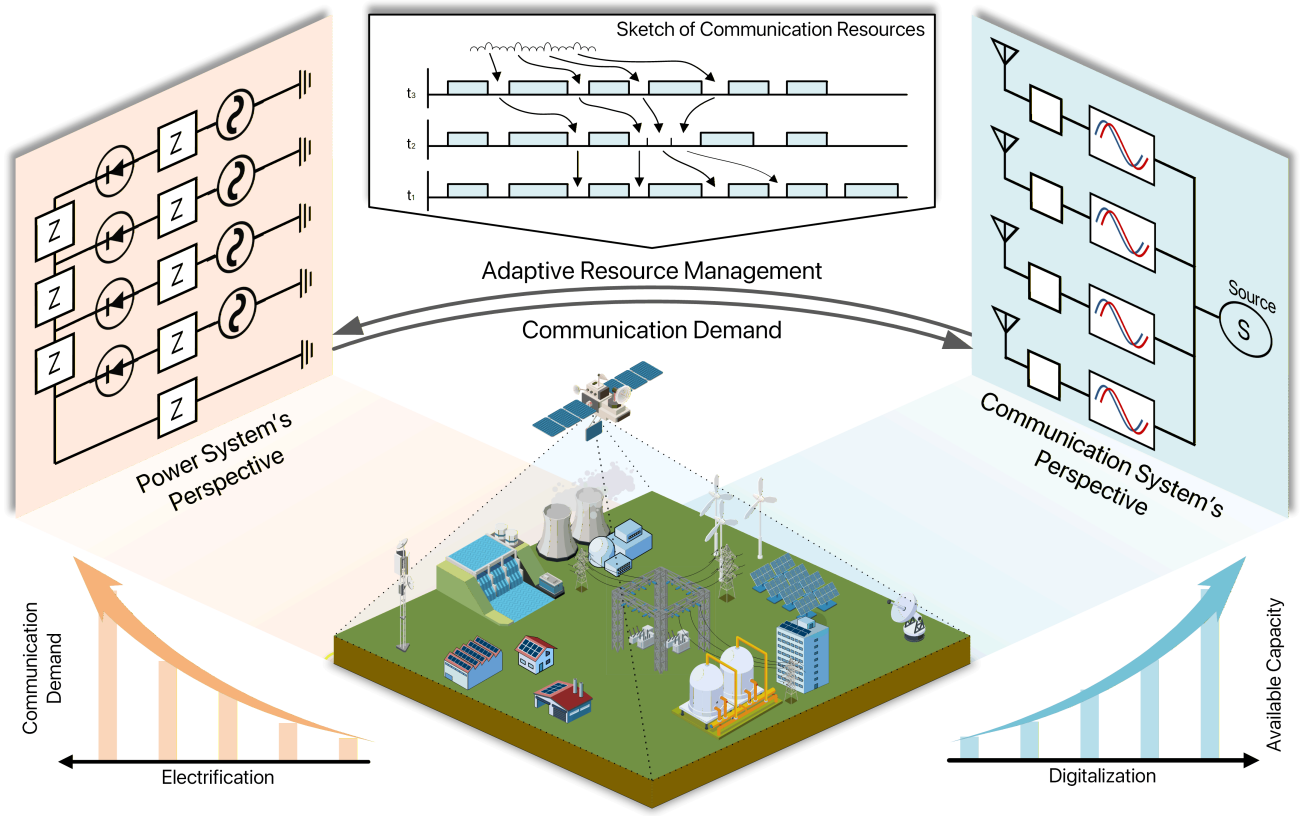



Fig. 1. The architecture of Cognitive Radio Empowered Smart Grid (CRESG).

economic efficiency in heterogeneous smart grid environments.

- To verify the effectiveness of the proposed CRESG framework in terms of cost reduction and stability maintenance, two representative smart grid scenarios are considered. The first involves satellite-aided control of offshore wind turbines, and the second focuses on remote control of distributed RERs. In addition, the simulation results demonstrate that CRESG can significantly reduce communication-control costs while maintaining system stability under varying network and environmental conditions, thereby enhancing the overall resilience and scalability of current and future smart grids.

The rest of the paper is organized as follows. The architecture of CRESG is presented in Section II. Subsequently, the theoretical framework is demonstrated in Section III, which integrates wireless communication resource management with smart grid control requirements. In Sections IV and V, two case studies on satellite-assisted control of offshore wind turbines and remote control of distributed RERs are provided, respectively, followed by the conclusion in Section VI.

## II. System Architecture: Entities, Links, and On-Demand Services

In constrast with traditional smart grids, where communication between DGs and the MC is typically established via wired connections, a CRESG adopts wireless communication links to coordinate the interaction. As illustrated in Fig. 1, this architecture represents a tight integration of a power system (the smart grid) and an information system (the wireless communication infrastructure), with data transmission delay $\tau$ serving as the critical coupling variable.

The two-level illustration specifically presents the integration of DGs, including wind turbines, photovoltaic panels, and hydrogen generators, with smart grid control and communication infrastructure. At the entity level, each DG is equipped with communication terminals and is electrically connected to an MC via power lines, while their communication is established through wireless channels. From the communication system's perspective, the MC acts as a centric server, and control signals (typically short packets) are dispatched by the connected BS, treating the DG terminals as user equipments. At the system level, latency is emphasized as the key cross-system interface, bridging the power system and the communication system. This architecture highlights the interdependence between energy generation, communication pathways, and distributed coordination in a CRESG.

In this architecture, control signals are typically transmitted as short packets, a design choice driven by the nature of power system operations and the constraints of wireless communication. These short packets are concise messages containing essential control information required for timely decision-making and distributed coordination among DG units, e.g., setpoints, command triggers, synchronization signals, or status acknowledgments. Unlike large stream data transmission (e.g., for video or firmware updates), these packets are usually a few

Authorized licensed use limited to: HUNAN UNIVERSITY. Downloaded on September 25,2026 at 04:35:22 UTC from IEEE Xplore. Restrictions apply.

bytes in size and are transmitted periodically or in response to events. The short-packet communication is particularly important in smart grid scenarios where low latency, high reliability, and minimal overhead are critical. For instance, commands issued by the BS to the communication terminals must be delivered within strict time constraints to ensure stable voltage/frequency regulation, load balancing, or fault response.

Moreover, the use of short packets aligns with emerging paradigms in URLLC within 5G and 6G networks, which are designed to support control-centric applications in smart grids. In the context of the architecture, the MC serves as the orchestrator that periodically transmits these short packets to the DG terminals. This control-driven communication, though lightweight in data volume, plays a critical role in maintaining system stability, ensuring synchronous operation across heterogeneous energy sources, and enabling the real-time interaction between the power and communication systems. In fact, the synchronization is necessary for the finite time stability of the smart grid as to be discussed in Section III.

The most significant distinction between a CRESG and a conventional wired-connected smart grid lies in the wireless communication architecture adopted between the MC and DGs. Unlike traditional smart grids, where wired links (e.g., fiber or Ethernet) are often used for local control, the CRESG leverages wireless channels to establish communication between the MC and DG terminals. This change introduces new design considerations related to latency, reliability, interference management, and spectrum efficiency, while simultaneously enabling greater flexibility, mobility, and ease of deployment in geographically distributed or infrastructure-limited environments especially for smart grid emergency maintenance.

A key implicit feature of the architecture is the bidirectional coupling between the power and communication systems. Stability metrics from the smart grid (e.g., voltage deviation, frequency nadir, settling time) feed back into the communication system's resource allocation decisions by constraining the transmission latency and error probability. Conversely, changes in spectrum availability, channel quality, or link reliability influence the received control signals at the power system and the corresponding grid QoS. This cross-system feedback loop ensures that both systems operate in a supportive manner, achieving a balance between cost, reliability, and stability.

To be specific, the transmission delay $\tau$ introduced by the wireless downlink directly impacts the control stability of the smart grid, which in turn influences the grid's operational and maintenance cost. At the same time, wireless communication resources themselves introduce an operational/economic cost, forming the second major component of the system's total cost, which consists of both the communication cost and the grid-side operational cost. To achieve both stability assurance and cost-efficiency, communication devices in the distributed network, i.e., the BS at the MC and the communication terminals at the DGs, must actively adapt their transmit power, bandwidth allocation, access strategy and other available communication resources. This enables the system to dynamically balance the trade-off between communication latency and power system stability, thereby minimizing the overall cost.

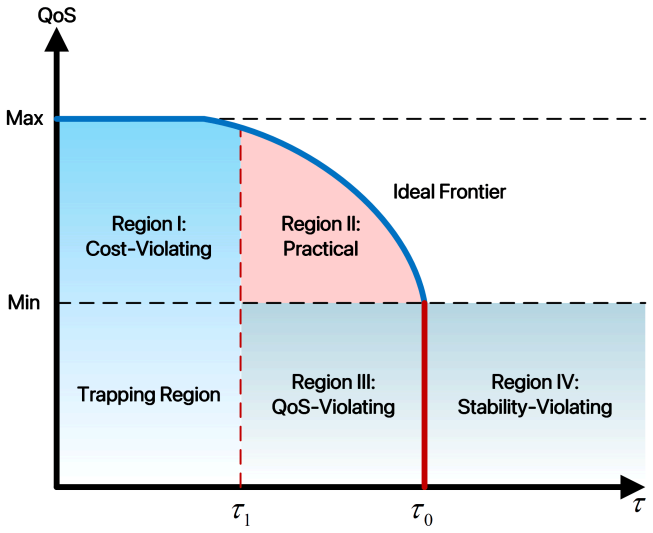



Fig. 2. Smart grid QoS degradation curve with respect to delay.

As illustrated in Fig. 2, the degradation of smart grid QoS in smart grid is significantly correlated with transmission delay $\tau$. The QoS curve begins at its maximum level (ideal performance) and gradually declines as delay increases, reflecting the diminishing effectiveness of timely control. The plot is partitioned into four distinct regions based on operational feasibility. Region I corresponds to the *cost-violating* domain, where ultra-low delays, although beneficial for QoS, induce excessive communication (and control) costs. Adjacent to this lies the *trapping region*, an infeasible phase that all engineers must carefully avoid during system design, as it offers neither cost-effectiveness nor performance reliability. Region II, situated between $\tau_1$ and $\tau_0$, represents the practical operating zone, where a balanced trade-off is achieved between QoS requirements and economic constraints. Note that the curve represents an *ideal performance frontier*, which is generally unattainable in practical implementations due to equipment limitaions, environmental uncertatinties, and the potential for human-induced errors. Between $\tau_1$ and $\tau_0$, Region III denotes a *QoS-violating* area in which the service level dips below acceptable thresholds despite being technically stable. Beyond $\tau_0$, the QoS drops sharply, defining Region IV, the *stability-violating* area, where delays are too long to support effective grid control, potentially endangering system reliability. This tradeoff highlights the necessity of maintaining communication delays within a constrained, feasible interval to uphold both performance and cost-efficiency in a CRESG.

In the context of large-scale renewable integration for future smart grids, the **long-tail effect** becomes increasingly evident, i.e., as RERs proliferate across geographically dispersed and low-density regions, the marginal cost of extending optical-fiber infrastructure to each site grows exponentially. For such distributed assets, especially those located in offshore, mountainous, or rural areas, the capital and maintenance costs of wired communication networks become economically unsustainable. Consequently, the communication demand of future smart grids can no longer be fully satisfied by fiber-based

Authorized licensed use limited to: HUNAN UNIVERSITY. Downloaded on September 25,2026 at 04:35:22 UTC from IEEE Xplore. Restrictions apply.

systems alone and must rely predominantly on wireless communication technologies. However, wireless communication resources are inherently limited, and their inefficient utilization can severely constrain grid-wide control performance. This challenge highlights the necessity of CRESG, which enables adaptive resource management to achieve cost-effective, reliable, and scalable communication for distributed RERs.

## III. Integrated Theoretical Modeling of Communication and Power Systems

We consider a MC equipped with wireless communication terminals, functioning as a base station in the context of communication systems, to serve smart grid of $N$ primary DGs, where the set is denoted by $\mathcal{N} = \{1, 2, \ldots, N\}$. The DGs are electrically interconnected via cables while wired communication is cut off [19]. Instead, communication is established over additive white Gaussian noise (AWGN) channels through wireless links from the MC to the DGs, operating under an multiple-in-single-out (MISO) configuration. Frequency division multiple access (FDMA) is employed to enable parallel downlink transmission from the MC to the DGs and avoid inter-user interference. Since the transmit information primarily consists of control signals, narrow-band communication is sufficient to satisfy system requirements. The bandwidth allocated to DG $k$ is denoted by $B_k$.

### A. Wireless Communication Model

The downlink channel is considered to experience large-scale path loss and small-scale fading. Moreover, both the line-of-sight (LoS) and Non-LoS (NLoS) transmissions are incorporated in the path loss model, where the LoS probability is expressed by a nonnegative function $P^{\mathrm{L}} : \mathbb{R}^+ \to [0, 1]$ of the transmission distance $d$ and other environment-dependent constant parameters. Correspondingly, the NLoS probability is written as $P^{\mathrm{N}} = 1 - P^{\mathrm{L}}$. Denote the large-scale LoS and NLoS path loss by $\xi^{\mathrm{L}}$ and $\xi^{\mathrm{N}}$, respectively. A general expression for the LoS/NLoS path loss can be given by

$$\xi^{v} = GA^{v}d^{-\alpha^{v}}, \quad v \in \{\mathrm{L}, \mathrm{N}\}, \tag{1}$$

where the superscript $v$ stands for LoS or NLoS transmission, $G$ is the antenna gain provided by the MC, $A^v$ stands for the path loss constant at the reference transmission distance 1m, $d$ denotes the transmission distance and $\alpha^v$ is defined as the LoS path loss exponent. Without loss of generality, the NLoS path loss $\xi^{\mathrm{N}}$ can be defined accordingly.

As for small-scale fading, we adopt the standard Nakagami-$m$ fading model [20] with unit spread parameter for the best generality. The probability density function (PDF) of the fading coefficient $\omega$ is given by

$$g_N(\omega) = \frac{2m^m\omega^{2m-1}}{\Gamma(m)}e^{-m\omega^2}, \quad \omega > 0, \tag{2}$$

where $m$ is the fading parameter depending on the environment and $\Gamma(\cdot)$ is the Gamma function. In particular, if $m \in \mathbb{N}^+$, the channel power gain $\omega^2$ is related to the gamma distribution, i.e., $\omega^2 \sim \text{gamma}(m, 1/m)$.

According to the downlink channel attenuation analysis, the received average SNR[1] of DG $k$ w.r.t. transmission modes is

$$\gamma_k = \frac{P_k^{\mathrm{L}}(\omega_k^{\mathrm{L}})^2\xi_k^{\mathrm{L}} + P_k^{\mathrm{N}}(\omega_k^{\mathrm{N}})^2\xi_k^{\mathrm{N}}}{N_0B_k}p_k, \tag{3}$$

where $p_k$ is the transmit power from the MC to DG $k$ and $N_0$ is the single-sided noise power spectral density. In addition, the subscript $k$ applies to transmission distance $d_k$, path loss constant $A_k^{\mathrm{L}}$ at the reference distance, path loss exponent $\alpha_k^{\mathrm{L}}$ and other environmental parameters.

In practice, smart grid control is highly sensitive to delays and necessitates URLLC [18] to ensure efficient and reliable operation. Given the characteristics of short packets in power control systems, an FBL regime is adopted in place of the classical Shannon capacity bound to more accurately reflect practical transmission constraints. For a discrete-time AWGN channel between the MC and DG $k$, the achievable data rate $\bar{R}_k$ in bits per channel use (bpcu) with (block) error probability $0 < \varepsilon_k < 1$, SNR $\gamma_k$, the number of (independent) channel uses $L_k$ (or equivalently the transmitted bits per symbol) has the following asymptotic expression [21]:

$$\bar{R}_k = \mathcal{C}_k - \sqrt{\frac{V(\gamma_k)}{L_k}}Q^{-1}(\varepsilon_k) + \frac{\log_2(L_k)}{2L_k}, \quad \text{(in bpcu)}, \tag{4}$$

where $Q(\cdot)$ is the Gaussian Q function (cumulative distribution function), i.e., $Q(x) := \int_x^\infty e^{-t^2/2}/\sqrt{2\pi}dt$ and $\mathcal{C}_k$ is the achievable Shannon capacity (in bpcu) for infinite-length codes without transmission error, which is expressed by

$$\mathcal{C}_k = \frac{1}{2}\log_2(1 + \gamma_k). \tag{5}$$

In addition, the channel dispersion $V(\gamma_k)$ is written as

$$V(\gamma_k) = \log_2^2 e \cdot \frac{\gamma_k(\gamma_k + 2)}{2(\gamma_k + 1)^2} = \frac{\log_2^2 e}{2}\left[1 - \frac{1}{(1 + \gamma_k)^2}\right]. \tag{6}$$

From the perspective of a continuous-time communication channel, the number of channel uses $L_k$, as a direct result of the Nyquist-Shannon sampling theorem, can be expressed by $L_k = 2B_k\tau_k$, where $B_k$ stands for the bandwidth and $\tau_k$ is the transmission latency. Moreover, the transmission rate in bits per second (bps) can be transformed from bpcu by $\hat{R}_k = 2B\bar{R}_k$ [22]. Therefore, an alternative expression for the data rate $R_k = \hat{R}_k/B$ in bps/Hz can be written as

$$R_k = \log_2(1 + \gamma_k) - \sqrt{\frac{2V(\gamma_k)}{\tau_kB_k}} + \frac{\log_2(2\tau_kB_k)}{2\tau_kB_k}. \tag{7}$$

Given the packet size $w_k$ (in bits), we have

$$w_k = \tau_kB_kR_k. \tag{8}$$

Therefore, it follows that

$$w_k = 2\tau_kB_k\mathcal{C}_k - \sqrt{2\tau_kB_kV(\gamma_k)}Q^{-1}(\varepsilon_k) + \frac{1}{2}\log_2(2\tau_kB_k).$$

[1] In this model, the received SNR is considered as a statistically averaged value. In practice, once the wireless communication devices are positioned, the transmission mode is determined to be either LoS or NLoS. Consequently, it is sufficient to set $P^{\mathrm{L}} = 0$ or $P^{\mathrm{N}} = 0$ accordingly, depending on the specific transmission scenario.

Authorized licensed use limited to: HUNAN UNIVERSITY. Downloaded on September 25,2026 at 04:35:22 UTC from IEEE Xplore. Restrictions apply.

In general, obtaining an analytical solution to the problem above, which involves solving for $\tau_k$ given $w_k$ and other parameters, is infeasible due to the complexity of the equation. However, in the high SNR case, i.e., $\mathcal{C}_k > 1$, an approximation can be made to significantly simplify the problem:

$$w_k \approx 2\tau_k B_k \mathcal{C}_k - \sqrt{2\tau_k B_k V(\gamma_k)} Q^{-1}(\varepsilon_k), \quad \mathcal{C}_k > 1. \tag{9}$$

A straightforward algebraic calculation gives

$$\tau_k = \frac{1}{2}\left(\frac{\zeta_k + \sqrt{\zeta_k^2 + 4w_k\mathcal{C}_k}}{2\sqrt{B_k}\mathcal{C}_k}\right)^2, \tag{10}$$

where $\zeta_k$ is short for $\sqrt{V(\gamma_k)}Q^{-1}(\varepsilon_k)$.

Based on the analysis above, an approximate closed-form relationship has been established among transmission delay $\tau_k$, SNR $\gamma_k$, bandwidth $B_k$ and error probability $\varepsilon_k$. In this article, we focus on the effects of communication system design on smart grid control, hence the time delays of backhaul link before the MC is treated as constant and not explicitly considered to simplify the discussion.

### B. Power Control Model

In contrast to a conventional power system that relies on wired connections, the smart grid considered in this section employs wireless links for communication. Therefore, the DGs can exhibit various feedback delays, and the corresponding physical system states can be asynchronous.

A general nonlinear time-delay smart grid model of DG $k$ for $k \in \mathcal{N}$ can be expressed by

$$\begin{cases} \dot{x}_k(t) = f_k(x_k(t), x_k(t-t_k)), & \forall t > 0, \\ x_k(t) = \phi_k(t), & \forall t \in [-\hat{T}, 0], \end{cases} \tag{11}$$

where $x_k(t) \in \mathbb{R}^r$ is the system state vector,[2] $\dot{x}(t)$ stands for the right-derivative of $x(t)$, $\phi_k : \mathbb{R} \to \mathbb{R}^r$ is a vector-valued initial condition function, $f_k : \mathbb{R}^r \times \mathbb{R}^r \to \mathbb{R}^r$ is a nonlinear continuous dynamical system governing the state evolution satisfying $f(0,0) = 0$, $t_k$ is the time delay between the past system state and the current control signals. Note that $t_k$ consists of the implicit transmission delay $\hat{t}$ of the backhaul link and the wireless transmission delay $\tau_k$ of the MC-DG link, i.e., $t_k = \hat{t} + \tau_k$. The preparation time $\hat{T}$ is selected such that $\hat{T} \geq \max\{t_1, t_2, \ldots, t_N\}$. Throughout the discussion, we assume that $\hat{t}$ is a constant irrelevant to the MC-DG link.

For the system (11), the classical finite-time stability analysis, which is based on a direct application of Lyapunov-Krasovskii theorem [23], yields the following result:

*Lemma 1:* [Proposition 4 in [24]]

Consider system (11) with uniqueness of solutions. If there exists $\delta > 0$ and a continuous functional $\mathbf{F} : \mathbf{C}_\delta \to \mathbb{R}$, $\epsilon > 0$, two functions $\lambda, \beta$ of class $\mathcal{K}$ such that $\dot{z} = -\beta(z)$ has a flow and for all $\phi_k \in \mathbf{C}_\delta$

1) $\lambda(\|\phi_k(0)\|) \leq \mathbf{F}(\phi_k)$,
2) $\dot{\mathbf{F}}(\phi_k) \leq -\beta(\mathbf{F}(\phi_k))$ with $\int_0^\epsilon \frac{dz}{\beta(z)} < +\infty$,

then the system (11) is finite-time stable with a settling time satisfying the inequality

$$T_0(\phi_k) \leq \int_0^{\mathbf{F}(\phi_k)} \frac{dz}{\beta(z)}. \tag{12}$$

Lemma 1 effectively provides the fundamental finite-time convergence guarantees for the smart grid control schemes discussed in the literature. The dependence of the settling time (12) on time delay $t_k$ is implicit, specifically through the functional $\mathbf{F}$. In fact, the aggregated power control system of all DGs for $t > 0$ can be expressed by

$$\dot{\mathbf{x}}(t) = f(\mathbf{x}(t), \mathbf{x}(t-t_1), \mathbf{x}(t-t_2), \ldots, \mathbf{x}(t-t_N)), \tag{13}$$

where $\mathbf{x}(t) \in \mathbb{R}^{rN}$ is the stacked vector of $\{x_k(t)\}_{k\in\mathcal{N}}$ and $f$ is the aggregated dynamical system.

### C. Optimization Problems

Suppose that the origin is the only point of the domain of $f$ defined in (13) satisfying $f(0, \ldots, 0) = 0$. According to [24, Remark 6], finite-time stability of the system can only be achieved if $t_1 = t_2 = \cdots = t_N$, i.e., the system dynamics (13) are determined by the current state and a single delayed input. Correspondingly, the wireless transmission delays are required to satisfy for some $\tau > 0$

$$\tau_1 = \tau_2 = \cdots = \tau_N = \tau. \tag{14}$$

The constraint (14) is inherently satisfied in a distributed cyber-physical system with wired communication connectivity within a local area. However, for wireless communication systems, it imposes additional requirements on aspects such as bandwidth allocation, transmit power control, access protocol design (for other types of modulation), among others.

In consideration of (14) and the constraints of *the communication system in this section*, the optimization problem involving the interaction between information (communication) and physical (power) systems can be formulated as

$$\begin{aligned} \min_{\{B_k\},\{p_k\}} \quad & \tau \\ \text{s.t.} \quad & \tau_1 = \tau_2 = \cdots = \tau_N = \tau, \\ & \sum_{k=1}^{N} B_k \leq B, \\ & p_k \leq p_{\max}, \ \varepsilon_k \leq \varepsilon_{\text{th}}, \quad \forall k \in \mathcal{N}. \end{aligned} \tag{15}$$

The constraints include feedback delay synchronization ($\tau_i = \tau_j, \forall i, j \in \mathcal{N}$), transmission reliability $(0, \varepsilon_{\text{th}}]$, power constraints of communication devices $[0, p_{\max}]$, and spectrum allocation subject to total bandwidth $B$.

The optimization problem (15), from the perspective of wireless communication, can be addressed by fully utilizing the available spectrum (i.e., $\sum_{k=1}^{N} B_k = B$) and maximizing the transmit power within permissible limits. Nevertheless, this approach also leads to increased costs associated with bandwidth rental and energy consumption for larger transmit power. Conversely, a reduction in transmission latency $\tau$ leads to a decrease in feedback delay, which in turn is correlated with a shorter settling time $T_0$. This implies a potential

[2]Without loss of generality, the origin is selected as the stable state. In fact, any nonzero stable state can be equivalently transformed into the origin through a coordinate translation.

Authorized licensed use limited to: HUNAN UNIVERSITY. Downloaded on September 25,2026 at 04:35:22 UTC from IEEE Xplore. Restrictions apply.

reduction in the operational expenditure required to maintain the stability of a smart grid. Based on the above analysis, the optimization problem on the costs of both communication and power systems can be formulated as

$$\begin{aligned} \min_{\{B_k\},\{p_k\}} \quad & \eta C_p + (1-\eta) C_e \\ \text{s.t. } & \tau_1 = \tau_2 = \cdots = \tau_N = \tau, \\ & \sum_{k=1}^{N} B_k \le B, \\ & p_k \le p_{\max},\ \varepsilon_k \le \varepsilon_{\text{th}}, \qquad \forall k \in \mathcal{N}, \end{aligned} \tag{16}$$

where $\eta \in [0,1]$ is the weight parameter, $C_p$ denotes the power generation cost associated with a settling time $T_0$, which is in turn determined by the transmission delay $\tau$, and $C_e(\cdot)$ represents the cost of communication resources required to realize transmission delay $\tau$. In principle, $C_p$ increases with $\tau$ reflecting the negative impact of larger delays on smart grid control performance, while $C_e$ typically increases as $\tau$ *decreases*, since lower-latency reliable communication requires more expensive resources. Accordingly, the optimization problem (15) can be viewed as a special case of the general form (16), wtih $\eta = 1$ and $C_p = \tau$. Note that both $C_p$ and $C_e$ may represent either economic costs (e.g., communication service fees, electricity generation costs) or physical metrics (e.g., time, energy consumption).

*Remark 1:* The theoretical framework proposed in this section is fundamental and can be readily extended to incorporate additional (or remove some) constraints in practical engineering applications (e.g., remote control of wind turbines, photovoltaic panels and other genrators), based on which a specific example is provided in the next section.

In the context of URLLC, information queuing latency is widely recognized as a critical contributor to end-to-end delay. However, its stochastic behavior and dependence on higher-layer (e.g., link-layer and application-layer) traffic dynamics make it less tractable within the scope of this study. In contrast, transmission latency can be more effectively optimized through physical-layer design. Therefore, this work concentrates exclusively on reducing transmission latency, while a detailed investigation of queuing effects is left to our future work. In addition, it is worth noting that queuing latency can readily be incorporated into the CRESG framework by modeling it as part of the backhaul link delay.

## IV. Performance Evaluation 1: Economic Cost

In this section, we aim to answer the question: ***What economic benefit does CRESG provide over a conventional wired-communication smart grid?*** To achieve this, we evaluate the performance of the CRESG by applying it to address the remote control challenges of offshore wind turbines through the support of LEO satellite communication. The objective is to strike a balance between the economic cost of reliable, low-latency communication services and the potential cost savings in power generation achieved by reducing the smart grid's settling time. The workflow is illustrated in Fig. 3. An MC equipped with a satellite terminal operates as an amplify-and-forward BS serving $M$ distributed wind turbines (DWTs), of which the set is denoted by $\mathcal{M} = \{1, 2, \ldots, M\}$.

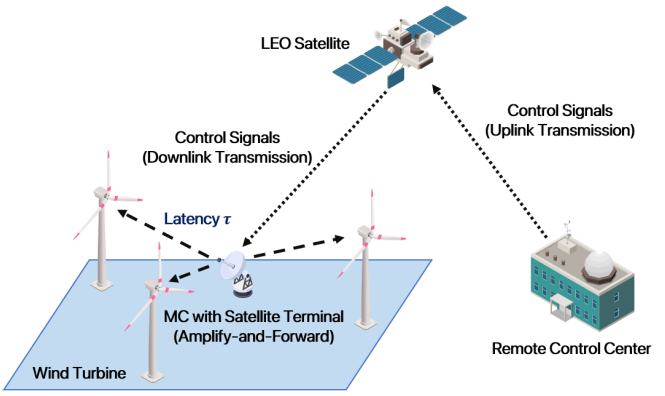



Fig. 3. Sketch of the emergency control workflow for offshore wind turbines supported by satellite communication.

### A. System Model and Problem Formulation

FDMA is used to enable the MC to simultaneously forward control signals to DWTs. Denote the total available bandwidth by $B$, and the bandwidth allocated to DWT $k$ by $B_k$, satisfying $\sum_{k=1}^{M} B_k \le B$. The MC uses multiple antennas to direct signals spatially to DWTs such that a distinct power level $P_k$ can be allocated for each beam toward DWT $k$. For simplicity, only the LoS path loss is considered, which is given by

$$\xi_k = \left(\frac{c}{4\pi d_k f_c}\right)^2, \tag{17}$$

where $f_c$ is the carrier frequency, $c$ denotes the speed of light, and $d_k$ represents the distance between the MC and DWT $k$.

To account for the multipath effects introduced by atmospheric refraction, ocean surface motion, and sea surface scattering in offshore environments, the small-scale fading of the MC-DWT wireless link is statistically modeled as Rayleigh fading, which is expressed by the following PDF:

$$f_{h_k}(h_k) = \frac{h_k}{\sigma_k^2} \exp\left(-\frac{h_k^2}{2\sigma_k^2}\right), \tag{18}$$

where $h_k$ is the instantaneous channel gain of MC-DWT $k$ link and $\sigma_k^2$ dentoes the scaling parameter. Given the AWGN channel, the received SNR of DWT $k$ is given by

$$\gamma_k = \frac{P_k |h_k|^2 \xi_k G_t G_k}{N_0 B_k}, \tag{19}$$

where $G_t$ is the antenna gain of the MC, $G_k$ represents the receiver antenna gain of DWT $k$ and $N_0$ denotes the single-sided noise power spectral density. Given the Rayleigh fading, the average SNR $\bar{\gamma}_k$ can be estimated by

$$\bar{\gamma}_k = \mathbb{E}[\gamma_k] = \frac{P_k \sigma_k^2 \xi_k G_t G_k}{N_0 B_k}. \tag{20}$$

Since contorl signals mainly comprises short packets, the FBL regime is applied. Under this regime, the achievable data rate $R_k$ (in bps/Hz) can be expressed by (7), where the average SNR $\bar{\gamma}_k$ is used and other variables are defined accordingly.

Authorized licensed use limited to: HUNAN UNIVERSITY. Downloaded on September 25,2026 at 04:35:22 UTC from IEEE Xplore. Restrictions apply.

The transmit data size for each DWT $k$ is denoted by $w_k$ and the transmission delay is $\tau_k = w_k/(B_k R_k)$.

Let the total bandwidth be $B = \sum_{k=1}^{M} B_k$. The total **available** bandwidth that can be provisioned by the network manager by $\bar{B}$. The rental cost of bandwidth for information transmission are represented by a differentiable and strictly increasing (possibly non-convex) function $C_{\rm b}(B)$, reflecting its growth with respect to the transmission load. The operational expenditure of the smart grid under transmission delay $\tau$ is given by a differentiable and strictly increasing (possibly non-convex) function $C_{\rm op}(\tau)$. Therefore, the total cost[3] $C_{\rm t}$ is expressed by (with slight abuse of notation)

$$C_{\rm t} = \alpha C_{\rm b}(B) + (1-\alpha) C_{\rm op}(\tau), \tag{21}$$

where $\alpha \in [0,1]$ is the weight parameter. Based on the above analysis, the optimization problem of hybrid-cost minimization can be formulated as

$$\mathcal{P}1: \min_{\{B_k,\tau_k\}} \ \alpha C_{\rm b}(B) + (1-\alpha) C_{\rm op}(\tau) \tag{22a}$$

$$\text{s.t. } \tau_1 = \tau_2 = \cdots = \tau_N = \tau \le \tau_{\rm th}, \tag{22b}$$

$$\sum_{k=1}^{M} B_k = B \le \bar{B}, \tag{22c}$$

$$\varepsilon_k \le \varepsilon_{\rm th}, \quad \forall k \in \mathcal{M}, \tag{22d}$$

where $\varepsilon_{\rm th}$ is the threshold of error probability required for reliable transmission and $\tau_{\rm th}$ represents the transmission latency requirement of smart grid control for stability. We assume that the transmit power $P_k$ of each DWT $k$ is given as a constant and all the variables must be positive.

*Remark 2:* The optimization problem (22) differs from classical communication system-involved optimization problems in two key aspects. First, the transmission latency is treated as a tunable time resource, that directly influences the error probability in the FBL regime. This contrasts with the conventional Shannon framework, where arbitrarily low error probabilities are assumed to be achievable regardless of latency. Second, the formulation naturally incorporates a tradeoff among economic costs of bandwidth, transmit power, and transmission latency (by influencing the operational expenditure of a smart grid) within a multi-objective optimization, as opposed to conventional formulations that usually focus on a single objective.

### B. Solution and Algorithm

The primary challenge in solving problem (22) arises from the non-convex constraint $\varepsilon_k = \varepsilon_k(B_k,\tau) \le \varepsilon_{\rm th}$, which introduces significant analytical complexity. To address this non-convex optimization problem, we derive a comprehensive analysis based on Lagrange multipliers and Karush-Kuhn-Tucker (KKT) conditions. To be specific, we consider the following augmented Lagrangian:

$$\mathcal{L} = C_{\rm t} + \sum_{k=1}^{M} \mu_k(\varepsilon_k - \varepsilon_{\rm th}) + \mu_{M+1}(B - \bar{B}) + \mu_{M+2}(\tau - \tau_{\rm th}),$$

[3]Note that the economic cost of energy consumption for transmission is negligible compared to the rental cost of bandwidth.

where $\mu_i$ for $i = 1, 2, \ldots, M+2$ is the Lagrange multiplier. Taking the partial derivatives with respect to the decision variables and using the KKT conditions give

$$\begin{cases} \dfrac{\partial \mathcal{L}}{\partial B_k} = \dfrac{\partial C_{\rm t}}{\partial B_k} + \mu_k \dfrac{\partial \varepsilon_k}{\partial B_k} + \mu_{M+1} = 0, \\ \dfrac{\partial \mathcal{L}}{\partial \tau} = \dfrac{\partial C_{\rm t}}{\partial \tau} + \mu_k \dfrac{\partial \varepsilon_k}{\partial \tau} + \mu_{M+2} = 0, \end{cases} \tag{23}$$

where $\psi_k := N_0/(\sigma_k^2 \xi_k G_t G_k)$ is short for the coefficient in (20) and the partial derivatives of $C_{\rm t}$ are expressed by

$$\frac{\partial C_{\rm t}}{\partial B_k} = \alpha C_{\rm b}'(B), \ \ \frac{\partial C_{\rm t}}{\partial \tau} = (1-\alpha) C_{\rm op}'(\tau), \tag{24}$$

where $h'(x)$ for a real-valued function $h$ represents the derivative. According to (8), given bandwidth $B_k$, latency $\tau$ and average SNR $\bar{\gamma}_k$, the error probability can be expressed by

$$\varepsilon_k = Q\left( \frac{1}{\sqrt{2\tau B_k V(\bar{\gamma}_k)}} \left[ 2\tau \mathcal{C}_k B_k + \frac{\log_2(2\tau B_k)}{2} - w_k \right] \right).$$

Define $H_k$ as

$$H_k := \frac{1}{\sqrt{2\tau B_k V(\bar{\gamma}_k)}} \left[ 2\tau \mathcal{C}_k B_k + \frac{\log_2(2\tau B_k)}{2} - w_k \right]. \tag{25}$$

Note that by definition

$$\mathcal{C}_k \sqrt{\tau B_k} - \frac{w_k}{\sqrt{\tau B_k}} = (\mathcal{C}_k - R_k)\sqrt{\tau B_k} > 0, \tag{26}$$

where $R_k$ is the achievable data rate, and hence $H_k > 0$. Next we derive the following expressions for the partial derivatives:

$$\begin{cases} \dfrac{\partial H_k}{\partial B_k} = \dfrac{1}{\sqrt{V(\bar{\gamma}_k)}} \left[ \mathcal{C}_k \sqrt{\dfrac{\tau}{2B_k}} + \dfrac{w_k}{2B_k\sqrt{2\tau B_k}} + O_k + \omega_k \right], \\ \dfrac{\partial H_k}{\partial \tau} = \dfrac{1}{\sqrt{V(\bar{\gamma}_k)}} \left[ \mathcal{C}_k \sqrt{\dfrac{B_k}{2\tau}} + \dfrac{w_k}{2\tau\sqrt{2\tau B_k}} + \tilde{O}_k \right], \end{cases}$$

where $O_k$, $\tilde{O}_k$ and $\zeta_k$ are short for

$$\begin{cases} O_k = \dfrac{1}{2B_k\sqrt{2\tau B_k}} \left( \dfrac{1}{\log 2} - \dfrac{\log_2(2\tau B_k)}{2} \right), \\ \tilde{O}_k = \dfrac{1}{2\tau\sqrt{2\tau B_k}} \left( \dfrac{1}{\log 2} - \dfrac{\log_2(2\tau B_k)}{2} \right), \\ \omega_k = \dfrac{\partial \mathcal{C}_k}{\partial B_k}\sqrt{2\tau B_k} - \dfrac{\partial V(\bar{\gamma}_k)}{\partial B_k} \dfrac{H_k}{2\sqrt{V(\bar{\gamma}_k)}}. \end{cases} \tag{27}$$

Moreover, we have

$$\frac{\partial V(\bar{\gamma}_k)}{\partial B_k} = -\frac{\log_2^2 e}{(1+\bar{\gamma}_k)^3} \frac{\bar{\gamma}_k}{B_k}, \tag{28a}$$

$$\frac{\partial \mathcal{C}_k}{\partial B_k} = -\frac{1}{2(1+\bar{\gamma}_k)\log 2} \frac{\bar{\gamma}_k}{B_k}. \tag{28b}$$

Therefore, the partial derivative of $\varepsilon_k$ w.r.t. $B_k$ is

$$\frac{\partial \varepsilon_k}{\partial B_k} = -\frac{1}{\sqrt{2\pi}} \exp\left\{ -\frac{H_k^2}{2} \right\} \frac{\partial H_k}{\partial B_k}, \tag{29}$$

and the derivatives with respect to $\tau$ is calculated accordingly. We continue to analyze the KKT condition in (23):

$$\frac{\partial \mathcal{L}}{\partial \tau} = \frac{\partial C_{\rm t}}{\partial \tau} + \mu_k \frac{\partial \varepsilon_k}{\partial \tau} + \mu_{M+2} = 0. \tag{30}$$

Recall that $\partial C_{\rm t}/\partial \tau$ is assumed to be strictly positive for all $\tau > 0$. In addition, the KKT conditions require the

Authorized licensed use limited to: HUNAN UNIVERSITY. Downloaded on September 25,2026 at 04:35:22 UTC from IEEE Xplore. Restrictions apply.

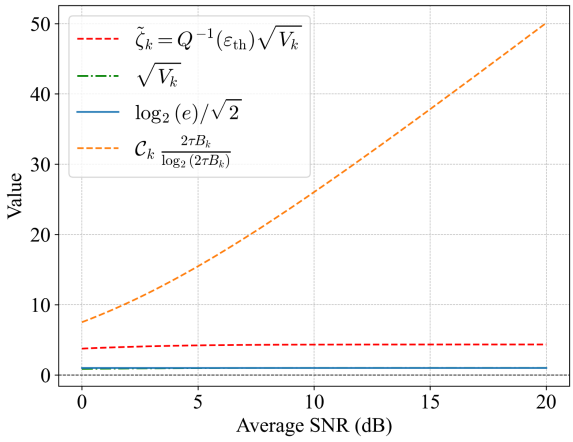



Fig. 4. The feasibility of high-SNR approximation with bandwidth $B_k$ = 100kHz, error probability $\varepsilon_{\text{th}}$ = 0.001% and latency $\tau$ = 1ms.

corresponding Lagrange multipliers $\mu_j$ to satisfy $\mu_j > 0$ for all $j \in \{1, 2, \ldots, M+2\}$. As a result, the complementary slackness condition $\mu_k(\varepsilon_k - \varepsilon_{\text{th}}) = 0$ implies that $\varepsilon_k = \varepsilon_{\text{th}}$ holds at the optimum for all $k \in \mathcal{M}$.

In practice, it is feasible to adopt the high-SNR assumption, i.e., to assume that $\bar{\gamma}_k$ is sufficiently large such that

$$\mathcal{C}_k = \frac{1}{2}\log_2(1+\bar{\gamma}_k) \gg \frac{\log_2(2\tau B_k)}{4\tau B_k}, \ \forall k \in \mathcal{M}. \tag{31}$$

Then we have for the optimum $\tau^*$ and $\{B_k^*, \bar{\gamma}_k^*\}$

$$Q^{-1}(\varepsilon_{\text{th}})\sqrt{V(\bar{\gamma}_k^*)} \approx \mathcal{C}_k\sqrt{2\tau^* B_k^*} - \frac{w_k}{\sqrt{2\tau^* B_k^*}}, \tag{32}$$

which by direct algebraic calculation yields

$$\sqrt{\tau^*} = \frac{Q^{-1}(\varepsilon_{\text{th}})\sqrt{V_k^*} + \sqrt{[Q^{-1}(\varepsilon_{\text{th}})]^2 V_k^* + 4\ w_k\mathcal{C}_k^*}}{2\sqrt{2B_k^*\mathcal{C}_k^*}}, \tag{33}$$

where $V_k^* := V(\bar{\gamma}_k^*)$ and $\mathcal{C}_k^* := \frac{1}{2}\log_2(1+\bar{\gamma}_k^*)$. Note that under the high-SNR approximation, the latency $\tau^*$ given by (33) is monotone decreasing w.r.t. $B_k^*$. To see this, we firstly consider the upper-bound estimate:

$$V_k^* = \frac{\log_2^2 e}{2}\left[1 - \frac{1}{(1+\gamma_k)^2}\right] \lessapprox \frac{\log_2^2 e}{2}. \tag{34}$$

Then we have the following high-SNR approximation:

$$\sqrt{\tau^*} \approx \frac{\kappa + \sqrt{\kappa^2 + 4w_k\mathcal{C}_k^*}}{2\sqrt{2B_k^*\mathcal{C}_k^*}}, \tag{35}$$

where $\kappa := Q^{-1}(\varepsilon_{\text{th}})\log_2 e/\sqrt{2}$. Given the transmit power $P_k$, the SNR $\bar{\gamma}_k^*$ is monotone decreasing w.r.t. $B_k^*$. The next step is to determine the monotonicity of the denominator. Indeed, it is sufficient to derive the real-valued positive function $h(x) = \sqrt{x}\log(1+1/x)$ for $x > 0$. Taking derivatives gives

$$\sqrt{x}h'(x) = \frac{1}{2}\log(1+x) - \frac{1}{1+x}, \tag{36}$$

where the right-hand side is clearly an increasing function and $h'(3) > 0$. Therefore, $\bar{\gamma}_k^* > 3$ (feasible in practice) ensures the denominator term $\sqrt{B_k^*\mathcal{C}_k^*}$ to be increasing w.r.t. $B_k^*$. Moreover, it can be deduced from (35) that

$$\frac{\kappa + \sqrt{\kappa^2 + 4w_i\mathcal{C}_i^*}}{2\sqrt{2B_i^*\mathcal{C}_i^*}} = \frac{\kappa + \sqrt{\kappa^2 + 4w_j\mathcal{C}_j^*}}{2\sqrt{2B_j^*\mathcal{C}_j^*}}, \forall i, j \in \mathcal{M}. \tag{37}$$

An alternative solution is to let $\sqrt{B_j^*\mathcal{C}_j^*} = \sqrt{B_i^*\mathcal{C}_i^*}$ and $w_j\mathcal{C}_j^* = w_j\mathcal{C}_j^*$, which indicates that $\sqrt{B_i^*}/\sqrt{B_j^*} = w_i/w_j$. Therefore, the occupied bandwidth can be represented by

$$B = \sum_{k=1}^{M} B_k = B_1\sum_{k=1}^{M}\frac{w_k^2}{w_1^2}, \tag{38}$$

which implies that the allocated bandwidth $B_1$ satisfies

$$B_1 \le \frac{w_1^2\bar{B}}{\sum_{k=1}^{M} w_k^2}. \tag{39}$$

The feasibility of the high-SNR approximation is illustrated in Fig. 4 under the typical parameter settings of bandwidth $B_k$ = 100kHz, error probability $\varepsilon_{\text{th}}$ = 0.001% and latency $\tau$ = 1ms. As can be observed, the curve of $\sqrt{V_k}$ closely overlaps with the horizontal line $y = \log_2(e)/\sqrt{2}$, indicating that the dispersion term becomes nearly constant when $\bar{\gamma}_k \ge 1$. Moreover, the capacity $\mathcal{C}_k$ exceeds $\log_2(2\tau B_k)/(2\tau B_k)$ by more than a factor of 7, which increases with respect to SNR, further validating the effectiveness of the approximation.

Via (33), the decision variables $\{B_k^*, \bar{\gamma}_k^*\}$ should satisfy

$$\frac{Q^{-1}(\varepsilon_{\text{th}})\sqrt{V_k^*} + \sqrt{[Q^{-1}(\varepsilon_{\text{th}})]^2 V_k^* + 4\ w_k\mathcal{C}_k^*}}{2\sqrt{2B_k^*\mathcal{C}_k^*}} \le \sqrt{\tau_{\text{th}}}. \tag{40}$$

Based on the above analysis, we have transformed the constraints $\varepsilon_k \le \varepsilon_{\text{th}}$, $B = \sum_{k=1}^{M} B_k \le \bar{B}$ and $\tau \le \tau_{\text{th}}$ into (33), (39) and (40), respectively. *Next we continue to discuss each specific case separately to maintain a feasible solution set $\mathcal{S}^*$ of the optimization problem (22).*

**Case 1: Interior Solution.** Let $\tau^* < \tau_{\text{th}}$ and $\sum_{k=1}^{M} B_k^* < \bar{B}$. The KKT complementary slackness conditions $\mu_{M+1}(B - \bar{B})$ and $\mu_{M+2}(\tau - \tau_{\text{th}}) = 0$ imply that $\mu_{M+1} = \mu_{M+2} = 0$. Then the optimal $(B_1^*, \tau^*)$ can be obtained by solving

$$\begin{cases} \sqrt{\tau^*} = \dfrac{\kappa + \sqrt{\kappa^2 + 4w_1\mathcal{C}_1^*}}{2\sqrt{2B_1^*\mathcal{C}_1^*}}, \\ \dfrac{\partial C_{\text{t}}}{\partial B_1}(B_1^*)\dfrac{\partial \varepsilon_1}{\partial \tau}(B_1^*, \tau^*) = \dfrac{\partial C_{\text{t}}}{\partial \tau}(\tau^*)\dfrac{\partial \varepsilon_1}{\partial B_1}(B_1^*, \tau^*). \end{cases} \tag{41}$$

It remains to verify that the pair $(B_1^*, \tau^*)$ satisfies $\tau^* < \tau_{\text{th}}$ and $B_1^* < w_1^2\bar{B}/\left(\sum_{k=1}^{M} w_k^2\right)$. If these conditions hold, the tuple $(\tau^*, \{B_k^*\})$ with $B_k^* = B_1^* w_k^2/w_1^2$ is appended to the solution set $\mathcal{S}^*$; otherwise, it is discarded.

**Case 2: Boundary Solution.** Let $\tau^* = \tau_{\text{th}}$. Firstly, we show that the equation (35) is solvable for $B_k$ given $\tau^* = \tau_{\text{th}}$. Use $q_k$ to represent the right-hand side of (35). It can be clearly observed that $q_k$ is continuous in and decreasing with respect to $B_k^*$, $\lim_{B_k^*\to\infty} q_k = 0$ and $\lim_{B_k^*\to 0} q_k = +\infty$. Therefore, there exists a unique solution to (35) for any $\tau_{\text{th}} > 0$ and the optimal bandwidth $B_k^*$ can be obtained by setting $\bar{\gamma}_k^* = P_k\sigma_k^2 G_t G_k/(B_k^* N_0)$. The next step is to verify whether the

Authorized licensed use limited to: HUNAN UNIVERSITY. Downloaded on September 25,2026 at 04:35:22 UTC from IEEE Xplore. Restrictions apply.

total allocated bandwidth satisfies the condition $\sum_{k=1}^{M} B_k^* \le \bar{B}$: if this condition holds, the solution $\{\tau_{\text{th}}, B_k^*\}$ is added to $\mathcal{S}^*$, otherwise it must be discarded.

**Case 3: Hybrid Solution.** Let $\tau^* < \tau_{\text{th}}$ and $\sum_{k=1}^{M} B_k^* = \bar{B}$. Each $B_k^*$ can be determined by

$$B_k^* = \bar{B}\frac{w_k^2}{\sum_{i=1}^{M} w_i^2}, \tag{42}$$

and the latency $\tau^*$ is determined by (35). If $\tau^* < \tau_{\text{th}}$, the tuple $(\tau^*, \{B_k^*\})$ is viewed as a feasible solution and added to $\mathcal{S}^*$.

**Algorithm 1** Iteration-Free Resource Allocation for Joint Communication and DWT Control Cost Minimization

**Setup:** The MC estimate/obtain the relevant system parameters for $M$ wireless downlink channels. Set the feasible solution set $\mathcal{S}^*$ to $\emptyset$ and determine $\alpha$, $\tau_{\text{th}}$, $\bar{B}$ and $\varepsilon_{\text{th}}$.

**Steps:**

1. Solve (41) for $\tau^*$ and $B_1^*$. Check the conditions:
$$\tau^* < \tau_{\text{th}}, \quad B_1^* < \bar{B}\frac{w_1^2}{\sum_{k=1}^{M} w_k^2}.$$
If they are satisfied, add $(\tau^*, \{B_k^* = B_1^* w_k^2 / w_1^2\})$ to $\mathcal{S}^*$.
2. Set $\tau^* = \tau_{\text{th}}$ and solve (35) for $B_k^*$. If $\sum_{k=1}^{M} B_k^* \le \bar{B}$, append $(\tau^*, \{B_k^*\})$ to $\mathcal{S}^*$.
3. Set $B_k^* = \bar{B} w_k^2 / \left(\sum_{i=1}^{M} w_i^2\right)$ and determine $\tau^*$ by (35). If $\tau^* < \tau_{\text{th}}$, add $(\tau^*, \{B_k^*\})$ to $\mathcal{S}^*$.
4. Compare the value of the objective function corresponding to each solution in $\mathcal{S}^*$ and select the optimal one:
$$(\tilde{\tau}, \{\tilde{B}_k\}) = \arg\min_{(\tau, \{B_k\}) \in \mathcal{S}^*} C_{\text{t}}.$$

**Output:** Transmission time $\tilde{\tau}$ and bandwidth $\{\tilde{B}_k\}$.

The overall iteration-free algorithm to solve the optimization problem (22) is summarized in Alg. 1. The primary challenge arises from solving the nonlinear transcendental equations (35) and (41). Denote the computational complexity of solving (35) and (41) by $\Omega_s$ and $\Omega_p$. Therefore, the total computational complexity can be expressed by $\mathcal{O}(\Omega_s + \Omega_p + 3M)$, which is free of an iteration number term.

### C. Simulation Results

To evaluate the performance of the proposed itertaion-free cost optimal (Opt-Cost for short) algorithm, we consider an offshore wind power control scenario involving $M = 5$ DWTs. Each DWT has a different control data size $w_k$, randomly drawn from an integer range between 180 and 240 bits. The average SNR of each DWT is determined based on a fixed transmit power $P_k = P = 1$ W ($\forall k \in \mathcal{M}$) and a randomly sampled communication distance between 500 m and 3500 m. The total available bandwidth $\bar{B}$ is set to 150 kHz, with a carrier frequency $f_c$ of 22.36 MHz. Unless otherwise specified, the threshold for acceptable transmission latency is $\tau_{\text{th}} = 1$ ms and the threshold for acceptable error probability is set to $\epsilon_{\text{th}} = 0.001\%$ (the corresponding reliability is 99.999%), which are typical settings for URLLC. The single-sided noise power spectral density $N_0$ is set to $4 \times 10^{-21}$ W/Hz and both antenna gains ($G_t$ and $G_r$) are set to 10.

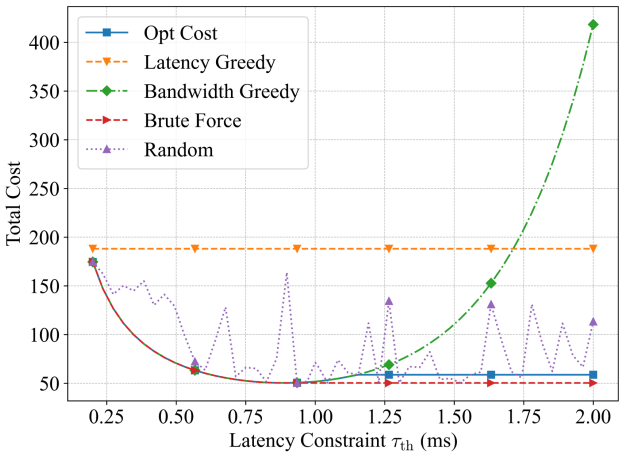



Fig. 5. Total cost versus varying $\tau_{\text{th}}$ ranging from 0.2 ms to 2 ms.

The total cost function includes two components: bandwidth rental cost and operational cost associated with transmission delay. The bandwidth cost is modeled as a linear function $C_{\text{b}}(B) = aB$ with $a = 2.5 \times 10^{-3}$ for bandwidth in Hertz, while the operational cost is modeled as an exponential function $C_{\text{op}}(\tau) = b(e^{\lambda\tau} - 1)$ with $b = 2$ and $\lambda = 3000$ for latency in seconds. The cost weight $\alpha \in [0, 1]$ controls the trade-off between the two. We evaluate the total cost under varying $\tau_{\text{th}}$ and $\alpha$ comparing Algorithm 1 with several baseline strategies. The four baselines are **latency-greedy**, **bandwidth-greedy**, **randomized allocation**, and **brute-force**. The latency-greedy scheme assigns the entire bandwidth budget to minimize latency, while the bandwidth-greedy strategy maximizes latency to reduce operational cost. The randomized scheme selects a feasible transmission latency randomly and determine the bandwidths by solving (35). The brute-force scheme provides the global cost-minimization strategy by grid search and serves as the ground truth.

As shown in Fig. 5, under fixed cost weight $\alpha = 0.5$, the total cost of Alg. 1 consistently outperforms all baselines (except the ground truth) across the full range of latency constraints $\tau_{\text{th}} \in [0.2, 2]$ ms. In particular, the proposed algorithm effectively captures the cost-latency trade-off, avoiding the steep cost increases encountered by the latency-greedy baseline at low $\tau_{\text{th}}$, and the instability or infeasibility of the randomized method. Notably, for near $\tau_{\text{th}} = 1.18$ ms, our algorithm achieves the lowest cost and comparable performance w.r.t. the ground truth by adaptively identifying a sweet spot where operational and bandwidth costs are optimally balanced. Due to the non-convexity of the optimization problem (22), developing a polynomial-time algorithm that guarantees globally optimal solutions is mathematically intractable, as such problems are known to be NP-hard.

Fig. 6 examines the influence of the cost weight $\alpha$ on the total cost, under a fixed latency constraint $\tau_{\text{th}} = 1$ ms. As $\alpha$ increases from 0 to 1, the importance of minimizing bandwidth cost increases. Opt-Cost dynamically adapts to this shift, adjusting $\tau$ and $\{B_k\}$ accordingly. The proposed algorithm

Authorized licensed use limited to: HUNAN UNIVERSITY. Downloaded on September 25,2026 at 04:35:22 UTC from IEEE Xplore. Restrictions apply.

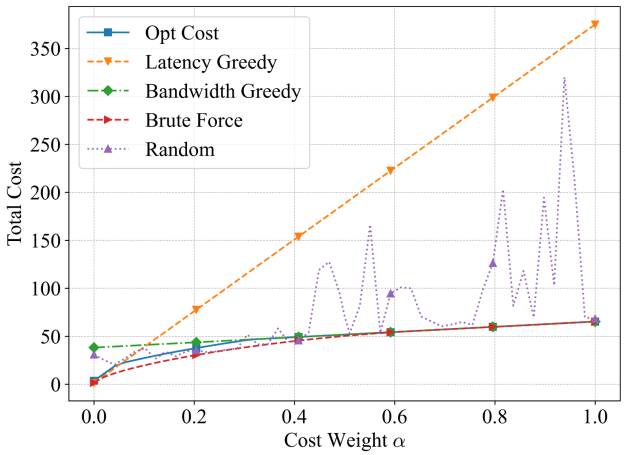



Fig. 6. Total cost versus varying $\alpha$ ranging from 0 to 1.

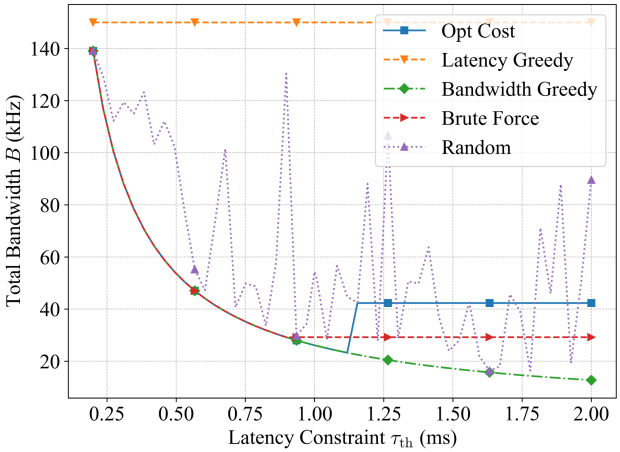



Fig. 8. Total occupied bandwidth versus varying $\tau_{\text{th}} \in [0.2, 2]$ ms.

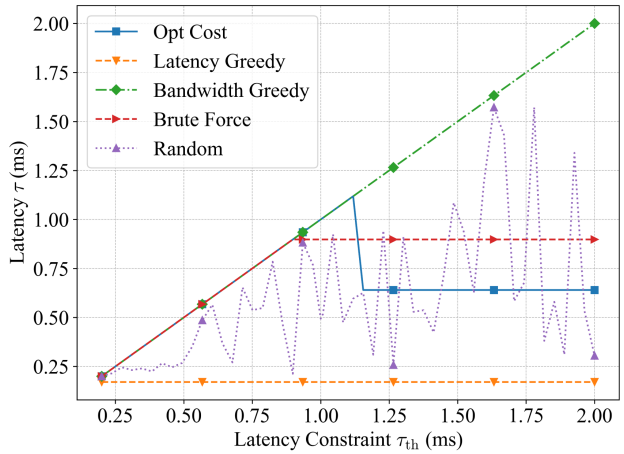



Fig. 7. Optimal transmission time versus varying $\tau_{\text{th}} \in [0.2, 2]$ ms.

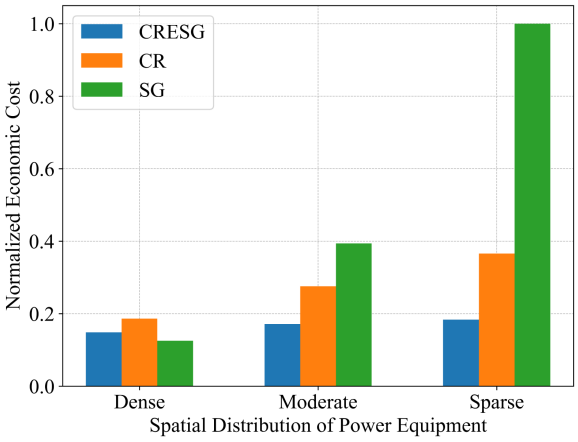



Fig. 9. Economic cost for different spatial distributions of power equipments.

maintains the lowest total cost across the full range of $\alpha$, validating its flexibility in heterogeneous cost environments.

Fig. 7 shows the optimal transmission time $\tau^*$ as a function of $\tau_{\text{th}}$, under fixed $\alpha = 0.5$. The proposed method consistently chooses transmission time values strictly less than $\tau_{\text{th}}$, except near saturation points, indicating its ability to actively trade off delay and bandwidth based on marginal cost. Moreover, the optimal transmission time of Alg. 1 remains lower than those of the two stable baselines except the latency-greedy method at the expense of a higher total occupied bandwidth (but still with lower cost), as illustrated in Fig. 8.

A notable turning point is observed in both Figs. 7 and 8 at approximately $\tau_{\text{th}} = 1.18$ ms. At this point, the proposed algorithm begins to adopt the solution derived from **Step 1**, as it becomes both feasible and more cost-effective than the solution obtained from **Step 2**, which enforces $\tau^* = \tau_{\text{th}}$. As a result, the algorithm shifts from a delay-saturated mode to a more balanced allocation, where the transmission time is reduced and bandwidth is reallocated accordingly. This shift leads to a visible change in the curvature of both the latency and bandwidth curves, highlighting the algorithm's ability to adaptively choose the most economical strategy.

Finally, we evaluate the economic cost associated with distinct spatial distributions of power-system equipments. Three representative deployment scenarios are examined: (i) dense, corresponding to urban environments in which equipments are tightly clustered and wireline communication infrastructure is highly pervasive; (ii) moderate, typical of rural locales where equipments are geographically dispersed and wireline connectivity is only partially available; and (iii) sparse, characteristic of remote renewable-rich regions in which installations are widely separated and fiber-optic backhaul is scarce or non-existent. We quantify the economic outlay for each spatial paradigm by comparing three candidate communication architectures: (i) a conventional smart-grid deployment that relies exclusively on wired connectivity (denoted SG); (ii) a cognitive-radio solution that minimizes over-the-air latency via appropriate spectrum management (denoted CR); and (iii) the proposed CRESG framework, which jointly optimizes communication and power system cost. The assessment is carried out under the dense, moderate, and sparse topologies defined above. The number of power equipments is set to 50, the latency constraint is fixed as 2 ms, the weight parameter $\alpha = 0.5$ and the total available bandwidth are 300 kHz, 450 kHz and 600 kHz, respectively. Fiber cost is estimated

Authorized licensed use limited to: HUNAN UNIVERSITY. Downloaded on September 25,2026 at 04:35:22 UTC from IEEE Xplore. Restrictions apply.

at 0.5 USD per meter amortized over a 30-year economic lifetime, then the average cost turns out 0.0167 USD/m per year. The other parameters remain unchanged. As illustrated in Fig. 9, SG achieves the lowest cost in dense regions because the cost of fiber optic cables is low and existing fiber-rich infrastructure immunizes it against disturbance-induced outages. When equipment density falls, however, the cost of new fiber drives SG expenditure sharply upward. CRESG, by contrast, sustains the minimum outlay for moderate and sparse topologies while remaining cost-competitive with SG in dense urban deployments. Analyzing the growth rates reveals that the cost of SG rises exponentially, CR increases linearly, whereas CRESG demonstrates a markedly slower, sublinear trend, which highlights its superior scalability.

## V. Performance Evaluation 2: System Stability

In this section, we aim to answer the question: ***How does communication resource management influence smart-grid stability?*** To achieve this, we evaluate the performance of the CRESG by applying it to address the stability issues (e.g., frequency control, voltage regulation) of a distributed renewable power system established on a wireless communication network. The objective is to enhance system stability by reducing the transmission latency of AGC signals [11], which in turn is achieved by efficient management of communication resources. The workflow is illustrated in Fig. 3. An MC equipped with a wireless communication terminal operates as a BS actively serving $K$ distributed RERs (as users), of which the set is denoted by $\mathcal{K} = \{1, 2, \ldots, K\}$.

### A. System Model and Problem Formulation

The communication model of the CR empowered renewable power system follows the same configuration as that described in Section IV-A. For a measurable control system, its dynamics can be captured and linearized by a stochastic linear time-invariant (LTI) system [25]. To improve feasibility, a discrete model is adopted, which is obtained by uniformly sampling the continuous-time system and can be expressed as follows:

$$x_k(t+1) = A_k x_k(t) + S_k u_k(t) + n_k(t), \tag{43}$$

where the time horizon is $T$ and the discrete time instant $t \in \{0, 1, 2, \ldots, T\}$. Moreover, $x_k(t) \in \mathbb{R}^r$ represents the plant state vector of RER $k \in \mathcal{K}$ at time $t$, $\tau_k$ is the time delay, $u_k(t) \in \mathbb{R}^\ell$ is the control input and $n_k(t) \sim \mathcal{N}(0, \Sigma_k)$ stands for the random Gaussian disturbance with constant covariance matrix $\Sigma_k \in \mathbb{R}^{r\times r}$. Note that only the wireless transmission delay of control signals is considered in this section. In addition, $A_k \in \mathbb{R}^{r\times r}$ is the system dynamics matrix and $S_k \in \mathbb{R}^{r\times \ell}$ is the input matrix. We assume that the matrices $A_k$ and $S_k$ are full-rank for all $k$ such that the system is controllable and desired control objectives are achievable. To evaluate the performance, a linear quadratic regulator (LQR) cost function is adopted, which can be written as

$$\mathcal{J}_k = \mathbb{E}\left[x_k^\dagger(T) W_k x_k(T) + \hat{\mathcal{J}}_k\right], \tag{44}$$

in which $\hat{\mathcal{J}}_k$ is short for

$$\hat{\mathcal{J}}_k = \sum_{t=0}^{T-1} \left(x_k^\dagger(t) U_k x_k(t) + u_k^\dagger(t)_k u_k(t)\right), \tag{45}$$

where $\dagger$ represents matrix transpose and $W_k, U_k \in \mathbb{R}^{r\times r}$ and $\xi_k \in \mathbb{R}^{\ell\times\ell}$ are positive semidefinite matrices. According to the classical result [26, Proposition 3.1], a necessary condition for asymptotic stabilizability of a noiseless version of system (43) (i.e., $n_k(t) = 0$ for all $t$) is that the communication channel data rate $R_k$ satisfies $R_k \geq \sum_{\lambda(A_k)} \max\{0, \log|\lambda(A_k)|\}$, where $\lambda(A_k)$ represents the eigenvalue of the matrix $A_k$. This implicitly indicates that the asymptotic stability of (43) depends jointly on the data rate $R_k$ and the eigenvalues of $A_k$. Define the matrix $E_k$ as the solution to the Riccati equation

$$\begin{cases} E_k = U_k + A_k^\dagger (E_k - F_k) A_k, \\ F_k = E_k S_k (V_k + S_k^\dagger E_k S_k)^{-1} S_k^\dagger E_k. \end{cases} \tag{46}$$

Denote the minimum attainable LQR cost by $\hat{z}_k := \mathrm{tr}(\Sigma_k E_k)$ in the absense of communication constraints, where $\mathrm{tr}(\cdot)$ is the trace of a matrix. Correspondingly, at any LQR cost $z > \hat{z}_k$, the rate-cost function satisfies [27, Theorem 1]

$$\mathcal{R}(z) \geq \log|\det(A_k)| + \frac{r}{2}\log\left(1 + \frac{\hat{H}(n_k)|\det(F_k)|^{1/r}}{(z-\hat{z}_k)/r}\right),$$

where $\det(\cdot)$ denotes the determinant of a matrix. For a random vector $Y \in \mathbb{R}^r$ with PDF $f_Y(y)$, $\hat{H}(Y)$ stands for the entropy power, which can be expressed by

$$\hat{H}(Y) = \frac{1}{2\pi e}\exp\left(-\frac{2}{r}\int_{\mathbb{R}^r} f_Y(y)\log f_Y(y) dy\right). \tag{47}$$

A straightforward algebraic calculation yields

$$\hat{H}(n_k) = 1 + \frac{(\det(\Sigma_k))^{1/r}}{2\pi e}. \tag{48}$$

It should be noted that since a discrete-time control model is applied in this section, the achievable data rate is expressed in its "channel efficiency" counterpart (4). The rate-cost function $\mathcal{R}(z)$ provides a lower bound on the minimum necessary capacity (in bpcu) of the channel to maintain an LQR cost $z$. By replacing the number of channel uses $L_k$ by the multiplication of transmission latency $\tau_k$ and required bandwidth $B_k$, i.e., $L_k = 2\tau_k B_k$. We have the following relationship:

$$\bar{R}_k = \mathcal{C}_k - \sqrt{\frac{V(\gamma_k)}{2\tau_k B_k}} Q^{-1}(\varepsilon_k) + \frac{\log_2(2\tau_k B_k)}{4\tau_k B_k}, \text{ (in bpcu)},$$

where the other parameters are defined according to Section III. To ensure the control process is asymptotically stable, the data rate $\bar{R}_k$ in bpcu must satisfy $\bar{R}_k \geq \mathcal{R}(z)$ for every $z \geq \hat{z}_k$. In addition, the lower-bound of LQR cost can be written as

$$\mathcal{J}_k^* = \hat{z}_k + \frac{r\hat{H}(n_k)|\det(F_k)|^{1/r}}{\exp\left(\frac{2}{r}(\bar{R}_k \log 2 - \log|\det(A_k)|)\right) - 1}, \tag{49}$$

where the term "log 2" arises from the unit conversion between bits and nats. According to the control model (43), control signals are $r$-dimension real-valued vectors.

Authorized licensed use limited to: HUNAN UNIVERSITY. Downloaded on September 25,2026 at 04:35:22 UTC from IEEE Xplore. Restrictions apply.

Across all the RERs, the primary objective is to minimize a weighted LQR cost, which can be expressed by

$$\bar{\mathcal{J}} := \sum_{k=1}^{K} \alpha_k \mathcal{J}_k^*, \tag{50}$$

where $\alpha_k > 0$ for all $k \in \mathcal{K}$ and $\sum_k \alpha_k = 1$. Note that $\alpha_k$ can be interpreted as the importance factor of each RER, i.e., a larger one means a primary RER which contributes more significantly to the overall stability of the grid. In addition to minimizing the lower bound of the LQR cost, it is equally important to ensure that this bound is practically attainable, which can be achieved through the careful selection of a coding scheme. For a fixed data rate, an appropriate coding scheme can reduce the error probability, thereby improving the overall control performance. Although the detailed design of coding schemes lies beyond the scope of this article, the error probability can still be mitigated through the efficient management of communication resources. Accordingly, a constraint is imposed to limit the maximum error probability across all MC-RER links, i.e., $\varepsilon_k \le \varepsilon_{\text{th}}$ for all $k \in \mathcal{K}$.

In summary, the overall optimization problem, which jointly considers communication resource constraints and control performance, is formulated as follows:

$$\mathcal{P}2: \min_{\{B_k,\tau_k,P_k\}} \quad \bar{\mathcal{J}} \tag{51a}$$

$$\text{s.t. } \tau_1 = \tau_2 = \cdots = \tau_N = \tau \le \tau_{\text{th}}, \tag{51b}$$

$$\sum_{k=1}^{K} B_k \le B_{\text{th}}, \tag{51c}$$

$$P_k \le P_{\text{th}}, \ \forall k \in \mathcal{K}, \tag{51d}$$

$$\bar{R}_k > \log_2 |\det(A_k)|, \quad \forall k \in \mathcal{K}, \tag{51e}$$

$$\varepsilon_k \le \varepsilon_{\text{th}}, \quad \forall k \in \mathcal{K}, \tag{51f}$$

where $B_{\text{th}}$ denotes the total available bandwidth, $P_{\text{th}}$ is the maximum transmit power and $\tau_{\text{th}}$ is the threshold of transmission latency. The constraint (51b), which enforces identical transmission latency, follows directly from (14). Although a discrete-time communication model is considered in this section, it can be obtained by uniform sampling of the continuous-time system. Consequently, the constraint (14) remains applicable to the discrete-time model.

In fact, the problem ($\mathcal{P}2$) inherently involves conflicts between its interdependent decision variables. Take the error probability for example. The achievable data rate $\bar{R}_k$ is monotonically increasing with respect to the error probability $\varepsilon_k$, given other parameters fixed. Consequently, minimizing $\varepsilon_k$ leads to a reduced $\bar{R}_k$, which in turn increases the lower-bound $\mathcal{J}_k^*$ of the LQR cost. Therefore, it is generally intractable to simultaneously achieve both a minimum error probability and a minimum LQR cost, necessitating the characterization of the inherent communication-control tradeoff.Indeed, the above analysis naturally extends to heterogeneous power control models, where the state vectors of different RERs may have varying dimensions, i.e., the dimension of $x_k(t)$ is $r_k$ and $r_k \neq r_{k'}$ for some $k \neq k'$. This is because the lower bound of the LQR cost is a scalar-valued function, which remains compatible across systems with different state dimensions. In this section, we address the case where the numbers of transmitted bits vary across all MC-RER links, which differs from the problem considered in Section IV.

### B. Solution and Algorithm

Although the problem ($\mathcal{P}_2$) seems to be complicated, it can be significantly simplified by investigating the relationship among the decision variables, the objective and constraints. To be specific, we have the following lemma:

*Lemma 2:* ($\mathcal{P}2$) can be equivalently transformed into

$$\mathcal{P}3: \min_{\{B_k,\tau\}} \bar{\mathcal{J}}, \quad \text{s.t. } \tau \le \tau_{\text{th}}, \ \sum_{k=1}^{K} B_k \le B_{\text{th}}. \tag{52}$$

*Proof:* A direct observation regarding problem ($\mathcal{P}_2$) is that it can be equivalently formulated in terms of the decision variables $\{\bar{\gamma}_k, B_k, \tau\}$ instead of $\{B_k, \tau_k, P_k\}$, since $P_k$ can be uniquely determined from $\bar{\gamma}_k$ given $B_k$. Notice that $\mathcal{J}_k^*$ is monotonically decreasing with respect to the data rate $\bar{R}_k$. Therefore, it is sufficient to calculate the optimal allocation that maximizes $\bar{R}_k$ given fixed $B_k$ and $\tau$. In fact, a straightforward analysis yields $\frac{\partial \bar{R}_k}{\partial \bar{\gamma}_k} > 0$. Since there is no coupling among the transmit powers of different MC-RER links, the optimal power allocation is given by $P_k = P_{\text{th}}$ for all $k \in \mathcal{K}$. The same analysis still applies to the error probability $\varepsilon_k$ and it follows that the optimal error probability is given by $\varepsilon_k = \varepsilon_{\text{th}}$ for all $k \in \mathcal{K}$. ∎

According to the Shannon's theorem and achievable data rates under the FBL regime (56), the gap between Shannon capacity and the achievable rate can be reduced by increasing the transmission duration under a fixed bandwidth. Therefore, the optimal transmission latency can be given by $\tau^* = \tau_{\text{th}}$.

To solve the problem ($\mathcal{P}3$), we follow a similar procedure as Section IV and consider the augmented Lagrangian:

$$\mathcal{L} := \bar{\mathcal{J}} + \mu \left( \sum_{k=1}^{K} B_k - B_{\text{th}} \right), \tag{53}$$

where $\mu \ge 0$ is the nonnegative Lagrange multiplier. According to the definition of $\bar{\mathcal{J}}$, we have

$$\bar{\mathcal{J}} = \sum_{k=1}^{K} \alpha_k \mathcal{J}_k^*(B_k). \tag{54}$$

Therefore, the KKT conditions imply

$$\begin{cases} \dfrac{\partial \mathcal{L}}{\partial B_k} = \mu + \alpha_k \dfrac{\partial \mathcal{J}_k^*}{\partial B_k} = 0, \\ \mu \left( \displaystyle\sum_{k=1}^{K} B_k - B_{\text{th}} \right) = 0. \end{cases} \tag{55}$$

Based on the analsyis in Section IV and Fig. 4, the high-SNR approximation for the data rate is adopted, i.e.,

$$\bar{R}_k \approx \mathcal{C}_k - \frac{\log_2 e}{2} \sqrt{\frac{1}{\tau B_k}} Q^{-1}(\varepsilon_{\text{th}}). \tag{56}$$

For convenience of subsequent analysis, the relevant partial derivatives are derived as follows:

$$\frac{\partial \bar{R}_k}{\partial B_k} = -\frac{\log_2 e}{2(1+\bar{\gamma}_k)} \frac{\bar{\gamma}_k}{B_k} + \frac{\log_2 e}{4B_k} \sqrt{\frac{1}{\tau_{\text{th}} B_k}} Q^{-1}(\varepsilon_{\text{th}}), \tag{57a}$$

Authorized licensed use limited to: HUNAN UNIVERSITY. Downloaded on September 25,2026 at 04:35:22 UTC from IEEE Xplore. Restrictions apply.

$$\frac{\partial \mathcal{J}_k^*}{\partial \bar{R}_k} = -2\varphi_k \log 2, \tag{57b}$$

$$\frac{\partial \mathcal{J}_k^*}{\partial B_k} = \frac{\varphi_k}{B_k}\left[\frac{\bar{\gamma}_k}{1+\bar{\gamma}_k} - \frac{1}{2}\sqrt{\frac{1}{\tau_{\text{th}} B_k}} Q^{-1}(\varepsilon_{\text{th}})\right]. \tag{57c}$$

where $\theta_k > 1$ and $\varphi_k$ are short for

$$\theta_k := \exp\left\{\frac{2}{r}\left(\bar{R}_k \log 2 - \log|\det(A_k)|\right)\right\}, \tag{58a}$$

$$\varphi_k := \frac{\hat{H}(n_k)|\det(F_k)|^{1/r}\theta_k}{(\theta_k - 1)^2} > 0. \tag{58b}$$

To solve the equations, two cases are discussed separately to maintain a feasible solution set $\mathcal{S}^*$ of problem $\mathcal{P}3$.

**Case 1: Interior Solution.** Let $\sum_{k=1}^K B_k^* < B_{\text{th}}$. The KKT complementary slackness condition $\mu\left(\sum_{k=1}^K B_k^* - B_{\text{th}}\right) = 0$ implies that $\mu = 0$, which in turn by (55) indicates that $\frac{\partial \mathcal{J}_k^*}{\partial B_k^*} = 0$. Therefore, the optimal bandwidth allocation scheme $\{B_k^*\}$ can be obtained by solving for all $k \in \mathcal{K}$

$$\frac{\varphi_k}{B_k}\left[\frac{\bar{\gamma}_k}{1+\bar{\gamma}_k} - \frac{1}{2}\sqrt{\frac{1}{\tau_{\text{th}} B_k}} Q^{-1}(\varepsilon_{\text{th}})\right] = 0. \tag{59}$$

It remains to verify that $\{B_k^*\}$ satisfies $\sum_{k=1}^K B_k^* < B_{\text{th}}$. If the condition holds, it is appended to $\mathcal{S}^*$, otherwise discarded. We note that, for convenience, the case where $\sum_{k=1}^K B_k^* = B_{\text{th}}$ and $\frac{\partial \mathcal{J}_k^*}{\partial B_k} = 0$ is also incorporated into this scenario.

**Case 2: Boundary Solution.** Let $\sum_{k=1}^K B_k^* = B_{\text{th}}$. By definition, we have $\mu > 0$ (the case for $\mu = 0$ has been merged into the first scenario) and

$$\mu + \frac{\varphi_k \alpha_k}{B_k}\left[\frac{\bar{\gamma}_k}{1+\bar{\gamma}_k} - \frac{1}{2}\sqrt{\frac{1}{\tau_{\text{th}} B_k}} Q^{-1}(\varepsilon_{\text{th}})\right] = 0. \tag{60}$$

Since the above equation is transcendental and analytically intractable, it is infeasible to derive a closed-form solution (solve for $B_k$ given some fixed $\mu$). Instead, we apply the projected gradient descent (PGD) method, which has been proven to converge to locally optimal points for any scalar-valued lower-bounded differentiable objective function, given appropriate selection of step sizes [28]. Given the decision vector $\mathbf{B} = (B_1, B_2, \ldots, B_K)^\dagger \in \mathbb{R}^K$, the iterates of PGD update for all $t \in \mathbb{N}^+$ according to

$$\mathbf{B}_t = \text{proj}_{\mathcal{X}}\left[\mathbf{B}_{t-1} - \beta_{t-1}\nabla_{\mathbf{B}_{t-1}} \bar{J}\right], \tag{61}$$

where $\beta_t \geq 0$ for all $t \in \mathbb{N}^+$ is the step size and the operator $\text{proj}_{\mathcal{X}}[\cdot] \subset \mathcal{X}$ maps a vector to a set containing projections onto the space $\mathcal{X}$, which can be formally defined by

$$\text{proj}_{\mathcal{X}}[y] \triangleq \left\{x \in \mathcal{X} : \|y - x\| = \inf_{z \in \mathcal{X}} \|y - z\|\right\}. \tag{62}$$

In our case, the space $\mathcal{X}$ is an affine plane expressed by

$$\mathcal{X} := \{x \in \mathbb{R}^K : \mathbf{1}^\dagger x = B_{\text{th}}\}, \tag{63}$$

where $\mathbf{1} \in \mathbb{R}^K$ denotes the vector with all elements to be 1. Note that since $\mathcal{X}$ is a closed and convex set, the projection set $\text{proj}_{\mathcal{X}}[y]$ for any $y \in \mathbb{R}^K$ degenerates into a singleton. According to basic facts from linear algebra, we have

$$\text{proj}_{\mathcal{X}}[y] = y - \frac{\mathbf{1}^\dagger y - B_{\text{th}}}{K}\mathbf{1}, \quad \forall y \in \mathbb{R}^K. \tag{64}$$

**Algorithm 2** Adaptive Resource Allocation for Joint Communication and LQR Control Cost Minimization

**Setup:** The MC estimate/obtain the relevant system parameters for $K$ wireless downlink channels. Set the feasible solution set $\mathcal{S}^*$ to $\emptyset$ and determine iteration number $\mathcal{T}$, step size $\{\beta_t\}$, LQR control cost weight $\{\alpha_k\}$, latency constraint $\tau_{\text{th}}$, available bandwidth $B_{\text{th}}$ and error probability threshold $\varepsilon_{\text{th}}$.

**Steps:**

1. Set $\tau^* = \tau_{\text{th}}$ and solve (59) for $\{B_k^*\}$. Check the condition $\sum_{k=1}^K B_k^* \leq B_{\text{th}}$. If it is satisfied, add $(\tau_{\text{th}}, \{B_k^*\})$ to $\mathcal{S}^*$.
2. Set $\tau^* = \tau_{\text{th}}$ and apply PGD to $\mathbf{B}$ as (61) with number of total iterations $\mathcal{T}$. Add the result $(\tau_{\text{th}}, \{B_k^*\})$ to $\mathcal{S}^*$.
3. Compare the value of the objective function corresponding to each solution in $\mathcal{S}^*$ and select the optimal one:

$$(\tilde{\tau}, \{\tilde{B}_k\}) = \arg\min_{(\tau, \{B_k\}) \in \mathcal{S}^*} \bar{\mathcal{J}}.$$

**Output:** Transmission time $\tilde{\tau}$ and bandwidth $\{\tilde{B}_k\}$.

Therefore, another potential solution $\{B_k^*\}$ is added to $\mathcal{S}^*$.

In summary, the total procedure of the algorithm is provided in Alg. 2. The whole process involves solving $K$ nonlinear equations (with complexity $\mathcal{O}(K\Omega_s)$) and a PGD, i.e., the computational complexity can be expressed by $\mathcal{O}(K\Omega_s + \mathcal{T})$.

### C. Simulation Results

This subsection evaluates the stability performance of the CRESG using the default simulation parameters following [25] and Section IV. To be specific, the number of RERs $K = 10$, the dimension $r = 6$, the single-sided noise power spectral density $N_0 = 4 \times 10^{-21}$ W/Hz, $B_{\text{th}} = 150$ kHz, carrier frequency $f_c = 22.36$ MHz, the determinant of the control system noise $\det(\Sigma_k) = 1$ ($\forall k \in \mathcal{K}$), $\log|\det(A_k)| = 7.8 + 0.3k$, the distance between the MC and each RER is randomly sampled from a uniform distribution $\mathcal{U}(500\text{m}, 1500\text{m})$, antenna gains $G_t = G_r = 1$, $\tau_{\text{th}} = 1$ ms, $\varepsilon_{\text{th}} = 0.0001\%$, $P_{\text{th}} = 0.4$ W, $\alpha_k = 2(K + 1-k)/[K(K+1)]$, $\hat{z}_k = 0.06$ ($\forall k \in \mathcal{K}$) and $|\det(F_k)| = k^2$, where we adopt heterogeneous power control settings for different RERs. The number of iterations for Alg. 2 is given by $\mathcal{T} = 100$ and step size $\beta_t = 1/(t+1)$.

To provide a comprehensive performance comparison, three spectrum management (SM) strategies are evaluated: active SM, passive SM, and linear adaptation (linear adap). In the active SM strategy, spectrum and transmission-time resources are jointly optimized by Alg. 2 through the proposed CRESG framework, enabling adaptive allocation in response to real-time channel variations and control requirements. The passive SM approach adopts a static allocation scheme determined offline by averaging the total bandwidth, without real-time adjustment during execution. The linear adaptation method distributes bandwidth proportionally to the importance factors $\alpha_k$ of the individual RERs, which naturally applies to the case where importance factors are time-varying.

As depicted in Fig. 10, when the latency constraint is relaxed, the achievable data rate increases and the corresponding control cost decreases. This trend reflects the fundamental

Authorized licensed use limited to: HUNAN UNIVERSITY. Downloaded on September 25,2026 at 04:35:22 UTC from IEEE Xplore. Restrictions apply.

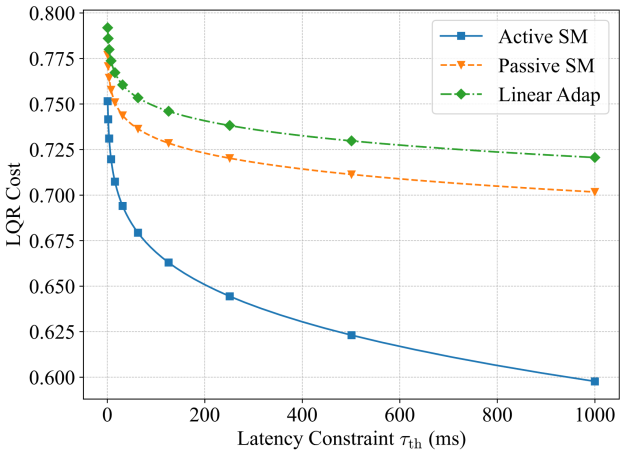



Fig. 10. Control cost versus varying $\tau_{\text{th}}$.

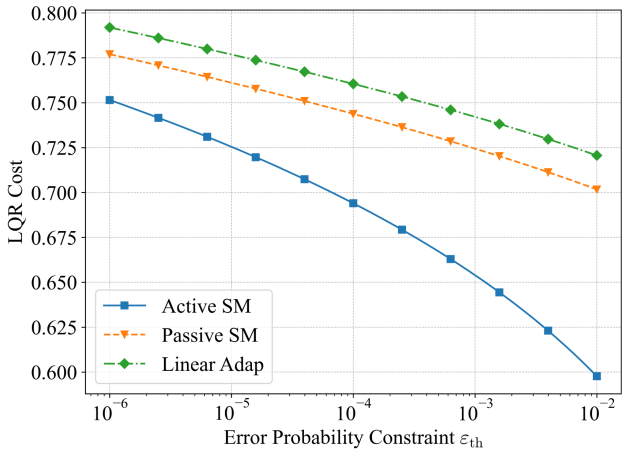



Fig. 11. Control cost versus varying $\varepsilon_{\text{th}}$.

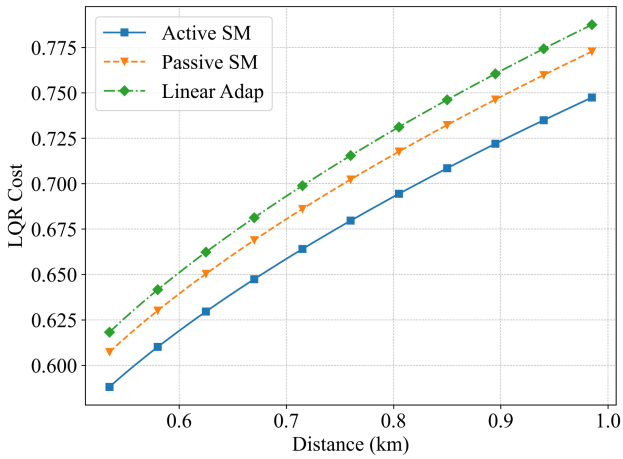



Fig. 12. Control cost versus varying transmission distance.

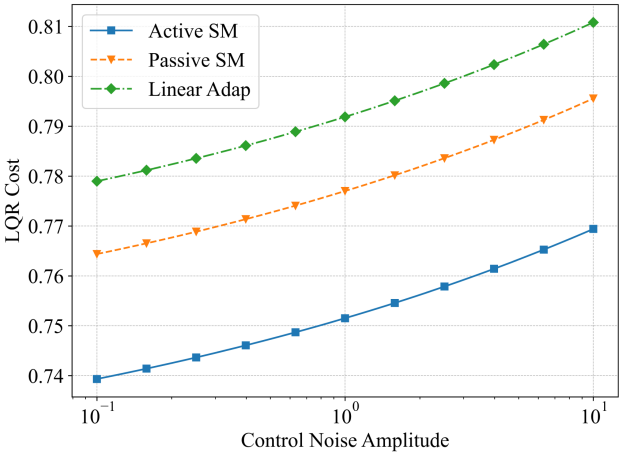



Fig. 13. Control cost versus varying control noise amplitude.

trade-off between delay tolerance and control performance. The active SM achieves the steepest cost reduction by exploiting the additional latency budget for appropriate bandwidth adaptation. The passive SM performs moderately, while the linear adaptation method remains least efficient. These results clearly indicate that adaptive latency response within the CRESG framework provides significant benefits for time-sensitive control of distributed RERs.

A looser reliability constraint $\varepsilon_{\text{th}}$ allows higher achievable data rates, thereby reducing overall control cost. As shown in Fig. 11, the active SM exhibits the most effective balance between transmission reliability and efficiency, while the passive SM and linear adaptation approaches lag behind. The increasing gap among the three schemes as $\varepsilon_{\text{th}}$ grows demonstrates that adaptive spectrum management under the CRESG framework plays a critical role in maintaining power system stability under varying reliability constraints.

To investigate the effects of transmission distance, we use different parameters for the uniform distribution with varying central distance. As illustrated in Fig. 12, when transmission distance increases, all spectrum-management strategies experience a gradual rise in LQR cost due to deteriorating channel quality. The active SM consistently outperforms the other two schemes by dynamically adjusting spectrum allocation in response to distance-induced signal degradation. The passive SM maintains intermediate performance, while the linear adaptation approach suffers the largest degradation at long distances. The results emphasize the necessity of adaptive spectrum coordination to mitigate performance loss in geographically extended communication scenarios.

To evaluate the effects of the control system noise on the proposed framework, we vary $\det(\Sigma_k)$ to adjust the noise intensity. As presented in Fig. 13, increasing the control-noise amplitude intensifies system fluctuations and inevitably raises the LQR cost for all methods. Nevertheless, the active SM maintains the lowest cost across the entire range, demonstrating its robustness to stochastic disturbances. The passive SM offers moderate resistance to noise, whereas the linear adaptation scheme exhibits the steepest cost increase as noise grows. These results verify that adaptive spectrum allocation enhances the resilience of the closed-loop system against random control perturbations.

Authorized licensed use limited to: HUNAN UNIVERSITY. Downloaded on September 25,2026 at 04:35:22 UTC from IEEE Xplore. Restrictions apply.

The trends across all the simulation results align closely with the theoretical analysis presented earlier. The proposed CRESG framework effectively bridges the communication-control coupling by adaptively managing spectrum resources. Compared with the passive SM and linear adaptation baselines, the active SM achieves consistently lower LQR costs and stronger robustness under diverse communication and control conditions. These findings validate the scalability and practicality of the CRESG-based active spectrum management for reliable operation of distributed RER systems.

## VI. Conclusion

This paper has proposed a CRESG architecture that integrates URLLC into distributed energy resource control through short-packet transmission under the FBL regime. A theoretical framework was established to model the coupling between wireless link dynamics and smart grid stability, and to formulate a cross-system optimization problem aimed at minimizing a hybrid cost function that captures both communication resource consumption and control-induced operational costs. To evaluate the performance of the CRESG, it is applied to satellite-assisted control of offshore wind turbines and remote control of RERs, demonstrating the effectiveness of the proposed framework in achieving low-latency, cost-efficient, and stable operation. Future research will focus on extending the framework toward deeper integration of communication and smart grid control, including circuit-level co-design, transient state analysis and more delicated communication protocol design, to further enhance system performance and adaptability in large-scale and heterogeneous smart grid environments.

As renewable generation (e.g., offshore wind farms, plateau photovoltaics, and clustered hydropower stations), device electrification, tremendous sensor networks and advanced 6G technologies (e.g., integrated satellite and terrestrial networks, and machine learning empowered wireless communication) continue to reshape modern power systems, an adaptive communication infrastructure is essential for the future smart grid. CRESG will not only serve as the cornerstone of future large-scale distributed renewable power infrastructures but also act as a crucial bridge linking the physical and information worlds. Ultimately, it embodies the emerging paradigm in which intelligent communication enables intelligent energy: *the smarter communication, the smarter power.*

## References


[1] M. B. Hossain, S. R. Pokhrel, and J. Choi, "Smart grid meets URLLC: A federated orchestration with improved communication for efficient energy resources management," *IEEE Internet Things J.*, vol. 10, no. 24, pp. 22440–22450, Dec. 2023.

[2] M. B. Hossain, S. R. Pokhrel, and J. Choi, "Orchestrating smart grid demand response operations with URLLC and MuZero learning," *IEEE Internet Things J.*, vol. 11, no. 4, pp. 6692–6704, Feb. 2024.

[3] N. Gholipoor, F. H. Aghdam, M. Rasti, and H. Zarini, "Strategic utilization of cellular operator energy storage for smart grid frequency regulation," *IEEE Trans. Smart Grid*, vol. 16, no. 5, pp. 3961–3975, Sep. 2025.

[4] R. C. Qiu et al., "Cognitive radio network for the smart grid: Experimental system architecture, control algorithms, security, and microgrid testbed," *IEEE Trans. Smart Grid*, vol. 2, no. 4, pp. 724–740, Dec. 2011.

[5] S. Alam, M. F. Sohail, S. A. Ghauri, I. M. Qureshi, and N. Aqdas, "Cognitive radio based smart grid communication network," *Renew. Sustain. Energy Rev.*, vol. 72, pp. 535–548, May 2017.

[6] S. Xiao, X. Ge, L. Ding, and D. Yue, "A bandwidth-conscious event-based control approach to secondary frequency regulation under vehicle-to-grid service," *IEEE Trans. Smart Grid*, vol. 15, no. 4, pp. 3739–3750, Jul. 2024.

[7] T. Yang, H. Li, S. Cai, and Y. Liu, "Distributed voltage control for microgrids against time-varying communication delay interference," *IEEE Trans. Smart Grid*, vol. 15, no. 3, pp. 2410–2423, May 2024.

[8] X. Chen et al., "Optimal two-timescale configuration of mobile edge computing with mixed energy supply," *IEEE Trans. Smart Grid*, vol. 15, no. 5, pp. 4765–4778, Sep. 2024.

[9] Z. Liu, Q. Wu, X. Shen, J. Tan, and X. Zhang, "Post-disaster robust restoration scheme for distribution network considering rerouting process of cyber system with 5G," *IEEE Trans. Smart Grid*, vol. 15, no. 5, pp. 4478–4491, Sep. 2024.

[10] H. Liao et al., "Timeliness-driven integrated sensing, transmission, computing, and control for power-communication coupling smart grid," *IEEE J. Sel. Areas Commun.*, vol. 43, no. 9, pp. 3134–3149, Sep. 2025.

[11] H. He et al., "Impact of communication time delay in a 5G network on frequency regulation performance of a high renewable energy penetrated power system," *IEEE Internet Things J.*, vol. 11, no. 14, pp. 24376–24388, Jul. 2024.

[12] H. Liao et al., "Integrated sensing, transmission and control for QKD-IoT empowered power-communication coupling smart grid," *IEEE Trans. Smart Grid*, vol. 16, no. 6, pp. 5514–5527, Nov. 2025.

[13] Y. Shen, Q. Zhou, Y. Wen, Z. Shuai, and Z. John Shen, "Integrated satellite-terrestrial network framework for next generation smart grid," *IEEE Trans. Smart Grid*, vol. 15, no. 5, pp. 5249–5252, Sep. 2024.

[14] T. Surinkaew and I. Ngamroo, "Communication-driven learning-based harmonic mitigation approach for grid-forming converters," *IEEE Trans. Smart Grid*, vol. 16, no. 6, pp. 4836–4853, Nov. 2025.

[15] Z. Lian, H. Yu, Y. Chen, M. Shahidehpour, and Q. Zhou, "Secure microgrid clusters under integrated satellite-terrestrial networks: A differential privacy-preserving control strategy," *IEEE Trans. Ind. Electron.*, early access, 2025, doi: 10.1109/TIE.2025.3594453.

[16] Y. Li, C. Lu, Y. Tang, C. Fang, and Y. Cui, "Dynamic control and time-delayed channel scheduling co-design for voltage control in active distribution networks," *IEEE Trans. Smart Grid*, vol. 15, no. 2, pp. 1837–1848, Mar. 2024.

[17] P. A. Hoeher, H. Beiranvand, and M. Liserre, "Information theoretical bounds for talkative power conversion," *IEEE Trans. Smart Grid*, vol. 16, no. 6, pp. 5655–5668, Nov. 2025.

[18] G. Durisi, T. Koch, and P. Popovski, "Toward massive, ultrareliable, and low-latency wireless communication with short packets," *Proc. IEEE*, vol. 104, no. 9, pp. 1711–1726, Sep. 2016.

[19] C. X. Rosero, M. Velasco, P. Martí, A. Camacho, J. Miret, and M. Castilla, "Analysis of consensus-based islanded microgrids subject to unexpected electrical and communication partitions," *IEEE Trans. Smart Grid*, vol. 10, no. 5, pp. 5125–5135, Sep. 2019.

[20] M. K. Simon and M.-S. Alouini, *Digital Communication Over Fading Channels*, 2nd ed., Hoboken, NJ, USA: Wiley, 2004.

[21] V. Y. F. Tan and M. Tomamichel, "The third-order term in the normal approximation for the AWGN channel," *IEEE Trans. Inf. Theory*, vol. 61, no. 5, pp. 2430–2438, May 2015.

[22] P. Popovski et al., "Wireless access in ultra-reliable low-latency communication (URLLC)," *IEEE Trans. Commun.*, vol. 67, no. 8, pp. 5783–5801, Aug. 2019.

[23] J. K. Hale and S. M. V. Lunel, *Introduction to Functional Differential Equations*, 1st ed., New York, NY, USA: Springer, 1993.

[24] E. Moulay, M. Dambrine, N. Yeganefar, and W. Perruquetti, "Finite-time stability and stabilization of time-delay systems," *Syst. Control Lett.*, vol. 57, no. 7, pp. 561–566, Jul. 2008.

[25] Z. A. Donbeh, M. Rasti, and S. K. Taskooh, "Active RIS-assisted communication and control co-design for LFC in smart grids," *IEEE Wireless Commun. Lett.*, vol. 14, no. 9, pp. 2887–2891, Sep. 2025.

[26] S. Tatikonda and S. Mitter, "Control over noisy channels," *IEEE Trans. Autom. Control*, vol. 49, no. 7, pp. 1196–1201, Jul. 2004.

[27] V. Kostina and B. Hassibi, "Rate-cost tradeoffs in control," *IEEE Trans. Autom. Control*, vol. 64, no. 11, pp. 4525–4540, Nov. 2019.

[28] Z. Xia, J. Du, C. Jiang, H. V. Poor, and Y. Ren, "Constrained optimization with low-bit gradients: A dynamical systems perspective," *IEEE J. Sel. Topics Signal Process.*, early access, 2025.


Authorized licensed use limited to: HUNAN UNIVERSITY. Downloaded on September 25,2026 at 04:35:22 UTC from IEEE Xplore. Restrictions apply.



**Zhaoyue Xia** (Member, IEEE) received the B.S. and Ph.D. degrees in electronic engineering from Tsinghua University, Beijing, China, in 2019 and 2025, respectively. He is currently an Assistant Professor with the College of Electrical and Information Engineering, Hunan University, Hunan, China. His research interests include power control and communication co-design, resource allocation, theory of non-convex optimization, and the applications of distributed optimization in the Internet of Things networks.



**Quan Zhou** (Senior Member, IEEE) received the B.S. and M.S. degrees from the Department of Electrical Engineering, Shanghai Jiao Tong University, Shanghai, China, in 2011 and 2016, respectively, and the Ph.D. degree from Illinois Institute of Technology, Chicago, IL, USA, in 2019. He is currently a Full Professor with the College of Electrical and Information Engineering, Hunan University, Changsha, China. His research interests include satellite internet and its applications in power systems, power control and communication co-design, space–air–ground integrated networks, and cybersecurity. He serves as an Associate Editor for IEEE TRANSACTIONS ON SMART GRID, IEEE TRANSACTIONS ON INDUSTRY APPLICATIONS, and IEEE POWER AND ENGINEERING LETTERS.



**Mohammad Shahidehpour** (Life Fellow, IEEE) received the Honorary Doctorate degree from the Polytechnic University of Bucharest, Bucharest, Romania, in 2009. He is currently a University Distinguished Professor, the Bodine Chair Professor, and the Director of the Robert W. Galvin Center for Electricity Innovation, Illinois Institute of Technology, Chicago, IL, USA. He is a member of U.S. National Academy of Engineering and a fellow of American Association for the Advancement of Science and the National Academy of Inventors.



**Zhikang Shuai** (Senior Member, IEEE) received the B.S. and Ph.D. degrees in electrical engineering from the College of Electrical and Information Engineering, Hunan University, Changsha, China, in 2005 and 2011, respectively. He was with Hunan University, as an Assistant Professor from 2009 and 2012, an Associate Professor in 2013, and a Professor in 2014. His research interests include power quality control, power electronics, and microgrid stability analysis and control. He received the 2010 National Scientific and Technological Awards of China, the 2012 Hunan Technological Invention Awards of China, and the 2007 Scientific and Technological Awards from the National Mechanical Industry Association of China. He is an Associate Editor of *CSEE Journal of Power and Energy Systems* and *Chinese Journal of Electrical Engineering*.

Authorized licensed use limited to: HUNAN UNIVERSITY. Downloaded on September 25,2026 at 04:35:22 UTC from IEEE Xplore. Restrictions apply.